

Ifremer

Ifremer
Unité de Recherche - Recherches et Développement Technologiques
Laboratoire Comportement des Structures en Mer
Marc Prevosto, Marc Le Boulluec

Ecole Centrale Nantes
Laboratoire de recherche en Hydrodynamique, Énergétique et Environnement Atmosphérique
Christian Klinghammer, Yves Perignon

Octobre 2015



Infragravity waves and moored floating structures



*Infragravity waves and moored
floating structures*

**M. Prevosto, M. Le Boulluec
C. Klinghammer, Y. Perignon**

**Ifremer
Ecole Centrale Nantes**

Abstract

Up to this day, design recommendations or practices for floating structures, such as DNVs RP-C205 and F205 for example, do not account for the existence of low frequency free Infragravity (IG) waves. These are low-frequency water waves which represent an additional excitation for (moored) floating structures.

In this study, the influence of free IG waves on moored floating structures response is investigated and compared to second-order low-frequency wave forces, as the standard low frequency excitation, for two selected important free IG events in 2013 and 2014 at the SEM-REV (Site d'Experimentation En Mer - Récupération de l'Energie des Vagues) test site near Le Croisic, Pays-de-la-Loire, France.

The wave forces and motion response for two example floater-mooringsystems are calculated and compared for the different frequency ranges separately and combined.

Using the latest developments in the wind-wave framework WAVE-WATCHIII®, e.g. the parameterized implementation of free IG sources at the reflecting boundaries, directional wave spectra including the low-frequency IG wave band are used.

This study has been conducted between November 2014 and October 2015 in the scope of the axis 7 «Sea motions and interaction with marine structures» of the cluster of Excellence LabexMER "A changing ocean".

Report

IG waves and moored floating structures

Version: 1.3
Date: 29/10/2015
Author: C. Klinghammer ECN/LHEEA
Supervisors: M. Prevosto IFREMER RDT-LCSM
Y. Perignon ECN/LHEEA

Index

- Symbols..... i
- 1 Summary 1
- 2 Introduction 2
- 3 Theory and methodology 3
 - 3.1 General methodology 3
 - 3.2 Conventions and assumptions 6
 - 3.3 Sum-over-diagonals method 8
- 4 Test Cases 10
 - 4.1 IG events 11
 - 4.2 Test floaters with mooring 15
 - 4.2.1 FSRU..... 15
 - 4.2.2 FPSO..... 18
- 5 Results 21
 - 5.1 Mechanical transfer function 21
 - 5.2 Motion LTF (Motion RAOs) 24
 - Force LTF (Force RAOs) 26
 - 5.3 Force QTF..... 28
 - 5.4 Low frequency wave forces 30
 - 5.5 Motion response 33
 - 5.6 Directional sensitivity 37
- 6 Summary and conclusions 44
- 7 Future work 48
- 8 References..... 51
- Appendix A - FPSO: Reproduction of available data. 52

Symbols

Symbol	Name	Unit
A	wave amplitude	[cm, m]
A_w	water plane area	[m ²]
C	(additional) Damping Matrix	[]
C_A	Radiation damping coefficient	[]
C_M	Added mass coefficient	[]
F	force, force amplitude	[N]
f	force, force amplitude	[N]
f	frequency	[Hz]
f_s	sampling frequency	[Hz]
GM_{xx}	metacentric height	[m]
g	gravitational acceleration	[m s ⁻²]
H	Wave height	[cm, m]
h	water depth	[m]
I	Identity matrix	[]
i	index, imaginary number	[]
j	index, imaginary number	[]
K_H	Hydrostatic stiffness matrix	[]
K	(additional) Stiffness matrix	[]
M	Mass-inertia matrix	[kg, kg·m, kg·m ²]
m	index	[]
n	index	[]
T	Wave period	[s]
X	Cartesian coordinate	[mm, cm, m]
Y	Cartesian coordinate	[mm, cm, m]
Z	Cartesian coordinate	[mm, cm, m]
α	Orientation angle floater	[°]
β	Wave incidence	[°]
η	Surface elevation	[m]
ρ	water density	[kg m ⁻³]
ω	angular wave frequency	[rad s ⁻¹]

1 Summary

Up to this day, design recommendations or practices for floating structures, such as DNVs RP-C205 and F205 for example, do not account for the existence of low frequency free Infragravity (IG) waves. These are low-frequency water waves which represent an additional excitation for (moored) floating structures.

In this study, the influence of free IG waves on moored floating structures response is investigated and compared to second-order low-frequency wave forces, as the standard low frequency excitation, for two selected important free IG events in 2013 and 2014 at the SEM-REV (Site d'Experimentation En Mer - Récupération de l'Energie des Vagues) test site near Le Croisic, Pays-de-la-Loire, France.

The wave forces and motion response for two example floater-mooring-systems are calculated and compared for the different frequency ranges separately and combined.

Using the latest developments in the wind-wave framework WAVEWATCHIII[®], e.g. the parameterized implementation of free IG sources at the reflecting boundaries, directional wave spectra including the low-frequency IG wave band are used.

This study has been conducted between November 2014 and October 2015 in the scope of the axis 7 «Sea motions and interaction with marine structures» of the cluster of Excellence LabexMER "A changing ocean".

2 Introduction

Moored floating structures may respond to wind, waves and current with motions on three different time-scales¹

- wave frequency (WF)
- low frequency (LF)
- high frequencies (HF), *not part of this study*

The largest wave loads on offshore structures take place at the same frequencies as the waves, causing wave frequency (WF) motions of the structure. To avoid large resonant effects, offshore structures and their mooring systems are often designed in such a way that the resonant frequencies are shifted well outside the WF range. The non-linear interaction of multi-chromatic waves with the hull results in second order LF and HF, as well as higher-order HF wave loads. Only the Second-order LF wave loads and the resulting steady drift and slow drift motions are considered in this study.

Infragravity waves are low-frequency water waves below the classical (gravity) WF-range, with frequencies $f_{IG}[\text{Hz}] \approx 0.0033$ to 0.03333 (Munk 1950), or respectively $f_{IG}[\text{Hz}] \approx 0.004$ to 0.04 or $T_{IG}[\text{s}] \approx 25$ to 250 (Rawat *et. al.* 2013). Part of these LF surface waves are related to the grouping of short period "wind waves" and travel as non-linear, 2nd-order "bound-waves" together with these wave groups in the open ocean. Once these wave groups are disturbed and their pattern is destroyed, for example as they reach the shore and start to break due to shoaling, the bound long waves are freed and become "free IG waves". As these very long waves do not break, they get almost fully reflected at the coast and depending on the bathymetry and reflection angle either get trapped on the shore and become "edge waves" or escape again towards the open sea as "leaky waves". Free IG waves represent an extra LF excitation for moored floating structures, such as FPSOs, Spars, TLPs and Semi-subs and therefore should be investigated. Table 2.1 shows typical natural periods of deep water floaters.

Floater mode	FPSO	Spar	TLP	Semi-sub
Surge	> 100	> 100	> 100	> 100
Sway	> 100	> 100	> 100	> 100
Heave	5 - 12	20 - 35	< 5	20 - 50
Roll	5 - 30	50 - 90	< 5	30 - 60
Pitch	5 - 12	50 - 90	< 5	30 - 60
Yaw	> 100	> 100	> 100	> 50 - 60

Table 2.1: Typical natural periods [s] of deep water floaters¹

¹ DNV-RP-C205, October 2010, p.64

3 Theory and methodology

In order to evaluate the importance of free IG waves to moored floating structures, the loads and responses at wave frequencies, standard second-order LF- and free IG frequencies are compared for different example floaters.

In recent publications (e.g. Ardhuin *et al*, 2014) the relation between storm-seas hitting the coast and strong free IG events has been investigated for a global and regional scale. These results were obtained using the wind-wave modeling software WAVEWATCHIII[®] (WW3, Tolman *et al.*, 2014), using a parameterized free IG source at the coastal boundaries. This novel approach gives a good estimation of directional wave spectra including the low-frequency free IG wave band for the site of interest for this study (SEM-REV test site).

Considering the strong theoretical differences in directions of sea-swell (WF and LF) and free IG waves, these directional wave spectra obtained with WW3 can be used to investigate the direction dependent loads and responses of a moored floater.

3.1 General methodology

The general approach in this study is to use the simulated directional wave spectra including the free IG wave band as input for a model to simulate in a first step the wave forces acting on a floater (for WF, LF, IG and combined) and in a second step to calculate the motion of the moored floater as response to these forces (again for WF, LF, IG and combined). Figure 3.1 shows the scheme for this model, which is similar to the motion computation in DIODORE[®]. This scheme of computation permits to calculate a-priori time series of forces (not knowing hull displacements) and so is much more faster than a time step by step calculation. (see Prevosto, 2010).

The first part, the linear free surface elevation $\eta(t)$, is calculated from a linear superposition of harmonic wave components with random Gaussian amplitudes defined by the one-sided spectral density $S_{\eta\eta}(\omega)$ (obtained with WW3)

$$\eta(t) = \Re \sum_{n=1}^N \sqrt{2S_{\eta\eta}(\omega_n)\Delta\omega} \cdot u_n e^{i\omega_n t} = \Re \sum_{n=1}^N \eta_n(\omega_n) e^{i\omega_n t} \quad 3.1$$

where u is a complex normal distributed random variable $u : N_N^C(0, I)$.

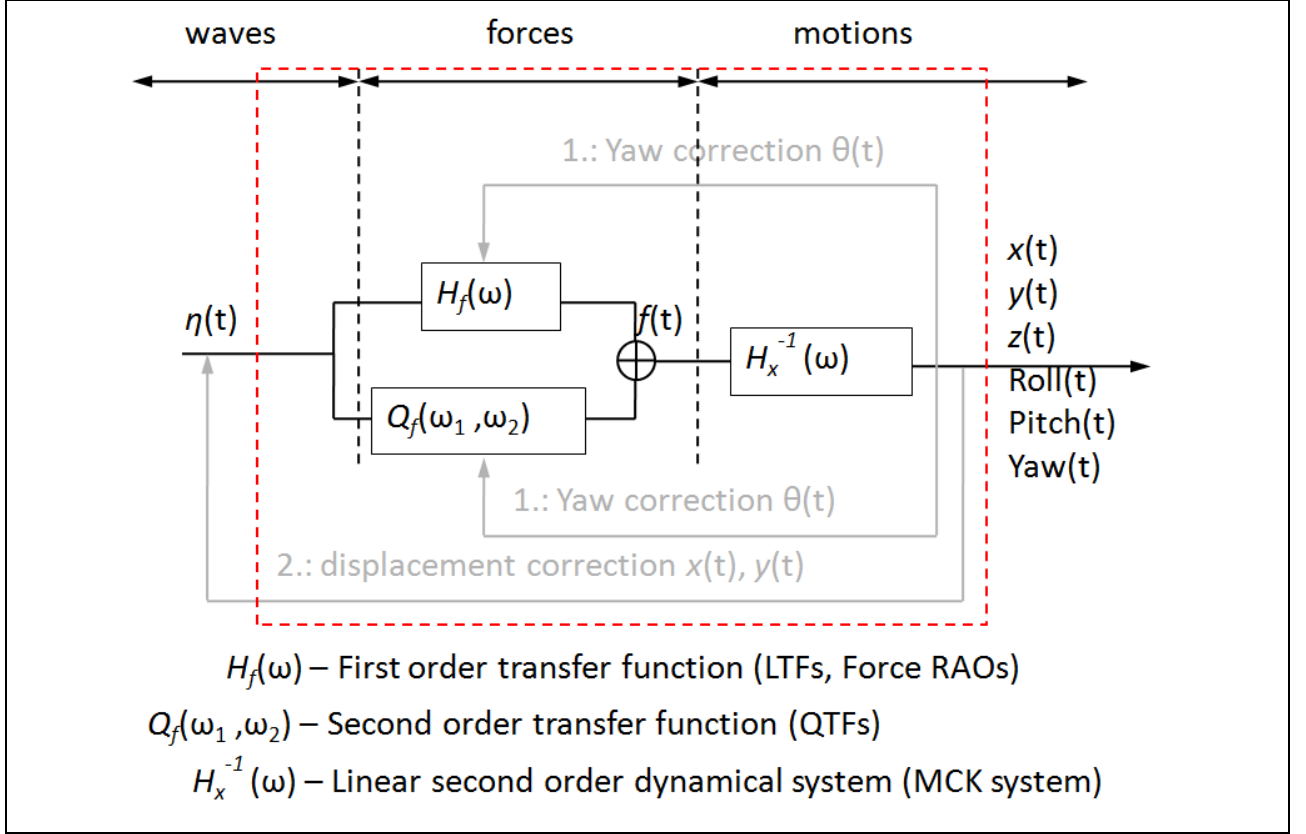


Figure 3.1: Force and motion time series calculation (scheme 1).

The second part of the model is the calculation of the forces acting on the hull of the floater. The forces as result to WF waves and IG waves are calculated by a first-order linear transfer function (H_f , LTF) or force-RAOs, while the second-order LF forces are calculated with a quadratic transfer function (Q_f , QTF).

Important: Because the free IG waves are considered a second-order wave effect and the scope of this study is only up to second-order forces and responses, the forces due to IG waves are calculated only with the LTF, neglecting the interaction of different IG frequency components.

Both, the LTF and QTF in this study are obtained by means of hydrodynamic analysis software (sea-keeping software). The low-frequency IG wave band requires the calculation of the radiation-diffraction terms for the entire frequency band including the IG band, which includes the structural resonant frequencies (see Table 2.1).

The time series for the forces can be calculated by

$$f(t) = \Re \sum_{n=1}^N H_f(\omega_n) \cdot \eta_n e^{i(\omega_n t)} + \sum_{n=1}^N \sum_{m=1}^N Q_f(\omega_n, -\omega_m) \eta_n \overline{\eta_m} e^{i(\omega_n - \omega_m)t} \quad 3.2$$

The third part of the model is the calculation of the motions as response to the forces. The mechanical transfer function for the 6DoF H_x^{-1} is obtained by solving the linear second-order differential equations of motion.

$$F(\omega) = [M + C_M] \ddot{X}(\omega) + [C_A + C_{extra}] \dot{X}(\omega) + [K_H + K_{extra}] X(\omega) \tag{3.3}$$

with mass-inertia matrix M , added masses C_M , radiation damping C_A , additional damping C_{extra} , hydrostatic stiffness matrix K_H and additional stiffness matrix K_{extra} (mooring).

As indicated in Figure 3.1, the model allows for a correction of large displacements and rotations for each time step. Without this correction the general methodology can be simplified in using only the bold black path as shown in Figure 3.2.

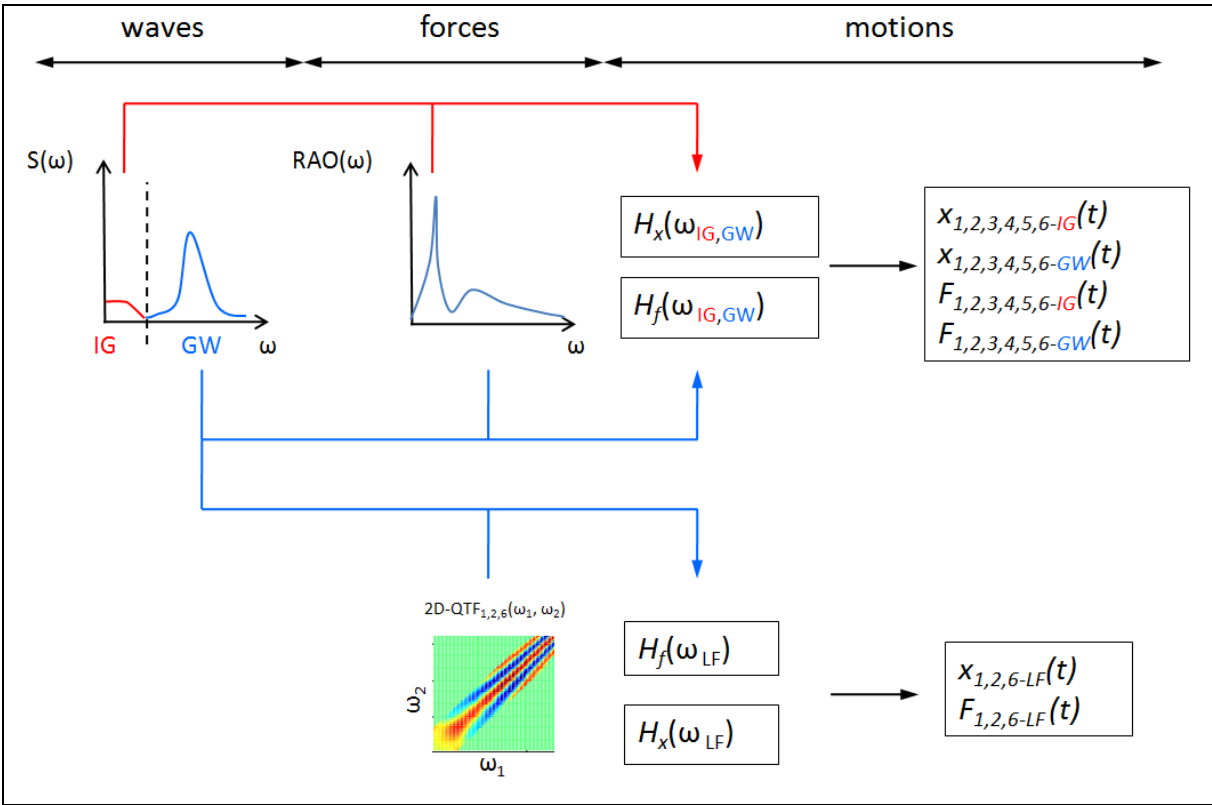


Figure 3.2: Force and motion time series calculation (scheme 2), $GW=WF$.

3.2 Conventions and assumptions

Before working with the WW3-IG spectra the directions have to be modified to match the conventions of the hydrodynamic analysis software DIODORE[®] and Bureau Veritas' HYDROSTAR[®]. The different directional conventions are indicated in Figure 3.3. The modifications are illustrated in Figure 3.4.

This CCW-oceanographic convention is used in this report from this point onward with the standard orientation of the floater being 0° (bow facing North).

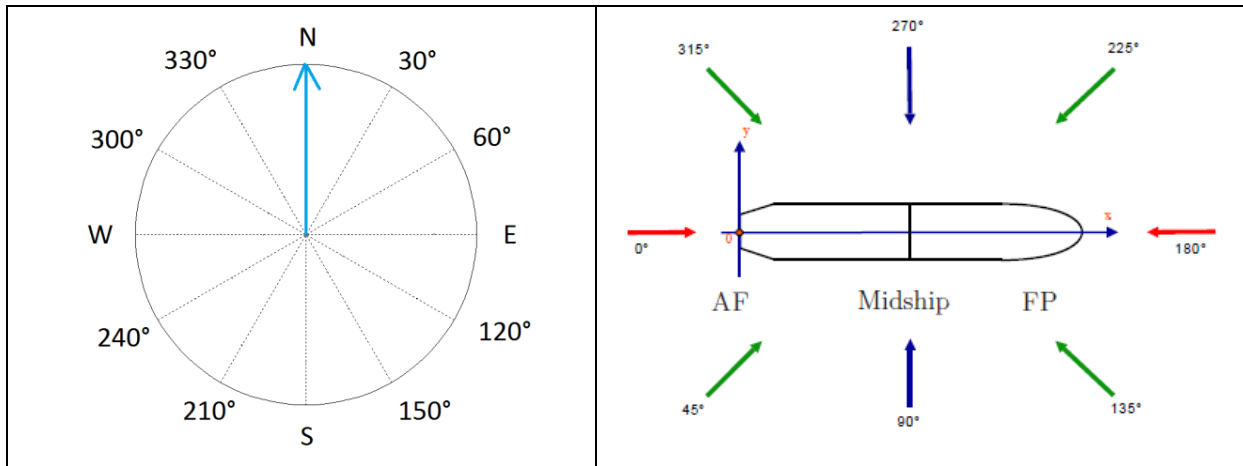


Figure 3.3: Left: WW3 directional wave spectra direction convention
Right: DIODORE/BV HYDROSTAR² direction convention.

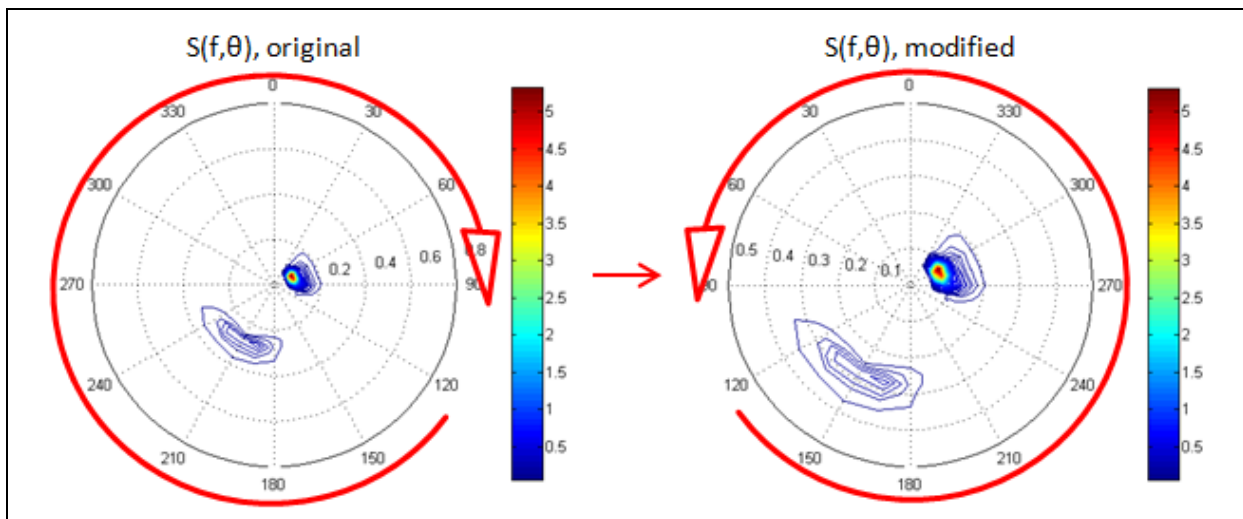


Figure 3.4: Modification of WW3-IG spectra directions (CW to CCW)

² HYDROSTAR FOR EXPERTS, USER MANUAL, BUREAU VERITAS, 04/2006

The second convention used in this report is the definition of the *Hermitian* QTF matrices, built with the output of HYDROSTAR®. The output for the complex valued QTF results is in the format; lines = wave frequency ω and columns = difference frequency $d\omega$ (see Figure 3.5, left).

The complex valued, *Hermitian*, square QTF matrix is constructed as shown in Figure 3.5 (from left to right), with the original HYDROSTAR results forming the upper triangle containing the difference frequencies $\omega_2 - \omega_1$. The lower triangle representing the difference frequencies $\omega_1 - \omega_2$ consists of the complex conjugates of the upper triangle. This convention is important for the time-series reconstruction of the *slow-drift* forces and motions. In the case of 4D-QTF or multidirectional QTF, there is one complex valued, *Hermitian*, square matrix for all possible combinations of two interacting directions.

The slow-drift forces can be calculated using 2D-QTF (Eq.3.4) or 4D-QTF (Eq. 3.5) for the case of multi-directional waves.

$$F(t) = \Re \left\{ \sum_{j=1}^N \sum_{k=1}^N QTF_{jk} a_j a_k^* \exp[-i(\omega_j - \omega_k)t] \right\} \quad 3.4$$

$$F(t) = \Re \left\{ \sum_{m=1}^M \sum_{n=1}^M \sum_{j=1}^N \sum_{k=1}^N QTF_{jkmn} a_{jm} a_{kn}^* \exp[-i(\omega_j - \omega_k)t] \right\} \quad 3.5$$

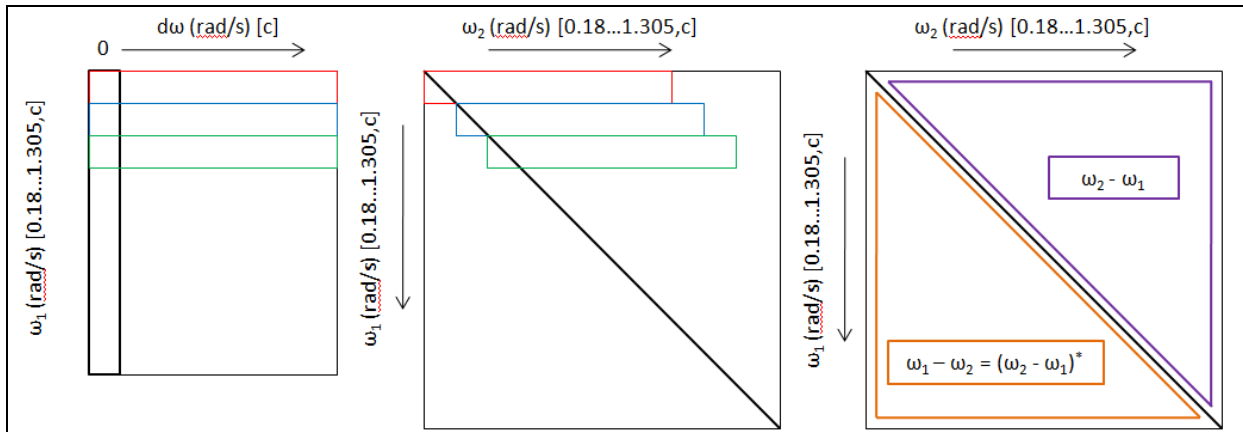


Figure 3.5: Construction of QTF matrices from HYDROSTAR® results.

3.3 Sum-over-diagonals method

In the case of 2D-QTF the slow-drift forces can be calculated very efficiently with a "sum-over-diagonals" method (Prevosto, 2010), avoiding the slow double-sum (see Eq. 3.4).

The method is presented in short as follows:

The second-order part of Eq. 3.2 can be rewritten as

$$F^{(2)}(t) = \sum_{\omega_n = \omega_{\min}}^{\omega_{\max}} \sum_{\omega_m = \omega_{\min}}^{\omega_{\max}} Q_f(\omega_n, -\omega_m) \eta(\omega_n) e^{j\omega_n t} \overline{\eta(\omega_m)} e^{-j\omega_m t} \quad 3.6$$

a 2D Fourier transform, and can be formulated as sum over the diagonals in summing over the super-diagonals

$$\sum_{\tau=0}^{\omega_{\max} - \omega_{\min}} \sum_{\tau=0}^{\omega_{\max} - \omega_{\min}} Q_f(\omega_n, -(\omega_n - \tau)) \eta(\omega_n) e^{j\omega_n t} \overline{\eta(\omega_n - \tau)} e^{-j(\omega_n - \tau)t} \quad 3.7$$

$$= \sum_{\tau=0}^{\omega_{\max} - \omega_{\min}} \left(\sum_{\omega_n = \omega_{\min} + \tau}^{\omega_{\max}} Q_f(\omega_n, -(\omega_n - \tau)) \eta(\omega_n) \overline{\eta(\omega_n - \tau)} \right) e^{j\tau t} \quad 3.8$$

$$= \sum_{\tau=0}^{\omega_{\max} - \omega_{\min}} R(\tau) e^{j\tau t} \quad 3.9$$

As Q is *Hermitian* and $\eta(-\omega_n) = \overline{\eta(\omega_n)}$,

$$R(-\tau) = \overline{R(\tau)} \quad 3.10$$

and the second-order forces can be written as a 1D inverse Fourier transform of $R(\tau)$. $R(\tau)$ is obtained by summation over the diagonals of the interpolated QTF. The interpolation is needed to match the frequency resolution for the time-series to be reconstructed.

$$R(\tau) = \sum_{\omega_n = \omega_{\min} + \tau}^{\omega_{\max} - \omega_{\min}} Q_f(\omega_n, -(\omega_n - \tau)) \eta(\omega_n) \overline{\eta(\omega_n - \tau)} \quad 3.11$$

and

$$F^{(2)}(t) = \sum_{\tau = -(\omega_{\max} - \omega_{\min})}^{\omega_{\max} - \omega_{\min}} R(\tau) e^{j\tau t} \quad 3.12$$

As each $R(\tau)$ is a summation over one diagonal, it is only necessary to store three interpolated diagonals. The scheme for the interpolation is shown in (Figure 3.6). The "black stars" represent the frequency discretization of the raw QTF from the sea-keeping software.

In a first step the diagonals are interpolated by calculating the main diagonal and the first super-diagonal on the interpolation frequency points. The result corresponds to the two first "red stars" diagonals.

Now the first interpolated super-diagonal (first "green stars" diagonal) is obtained by interpolating between the interpolated main and the first diagonal. $R(\tau)$ is calculated from this diagonal and the interpolated super-diagonal is erased from memory. The process continues in the same way for all the super-diagonals between the first "red stars" diagonals.

When this is done, $R(\tau)$ is calculated from the interpolated main diagonal and this diagonal is erased as well.

The process continues with a new "black stars" super-diagonal. With this procedure only three interpolated diagonals have to be stored in memory simultaneously (two red and one green).

As $R(-\tau) = \overline{R(\tau)}$, only the upper half of the QTF has to be processed. At the end, the second-order force time series $F^{(2)}(t)$ is calculated by inverse Fourier transform of $R(\tau)$.

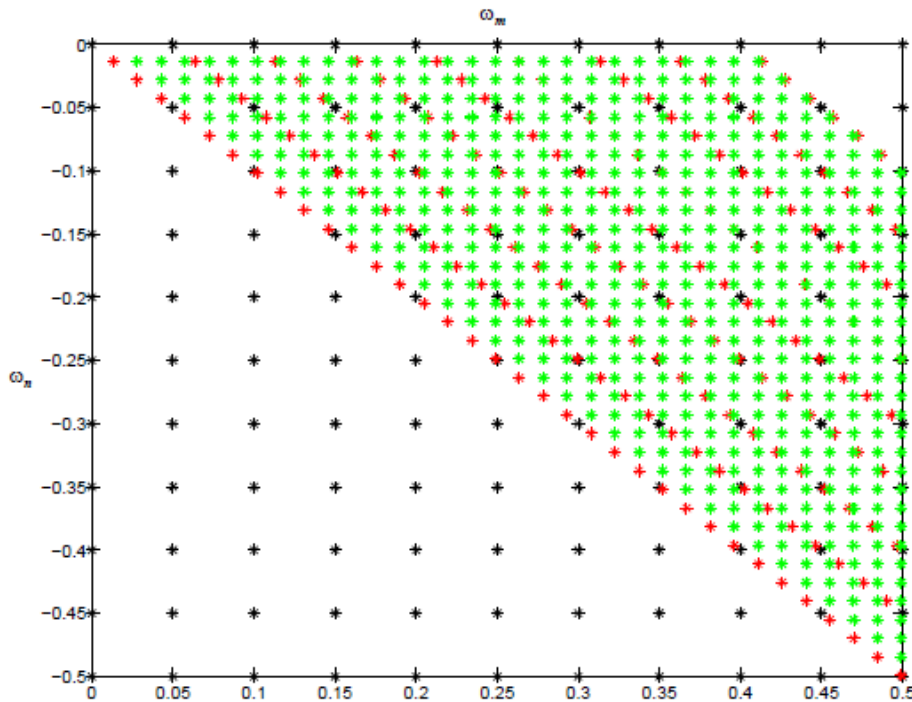


Figure 3.6: Scheme of QTF interpolation

4 Test Cases

The test cases for this study are two important free IG events, on 24/12/2013 and on 07/01/2014 at the SEM-REV location. For both dates the force and motion-response time-series are calculated for two generic example floaters with spread mooring (FSRU and FPSO).

The SEM-REV test site is situated on the French Atlantic coast on the Armorican shelf near Le Croisic, Pays-de-la-Loire. The exact location of its center is given³ as 2° 46.73' W - 47° 14.34' N. All the area of the Armorican shelf has been identified to show strong free IG events.

Figure 4.1 shows the locations of SEM-REV and the closest export node (W0027N472) from the WW3-IG calculations for 2013 (Rawat 2015), and new WW3-IG calculations for January 2014 done for this study by F. Arduin, using the same global grid with a 5° resolution.

The WW3-IG calculations for 12/2013 and 01/2014 were conducted with a constant water depth h , with $h = 45.71$ m at the W0027N472 node.

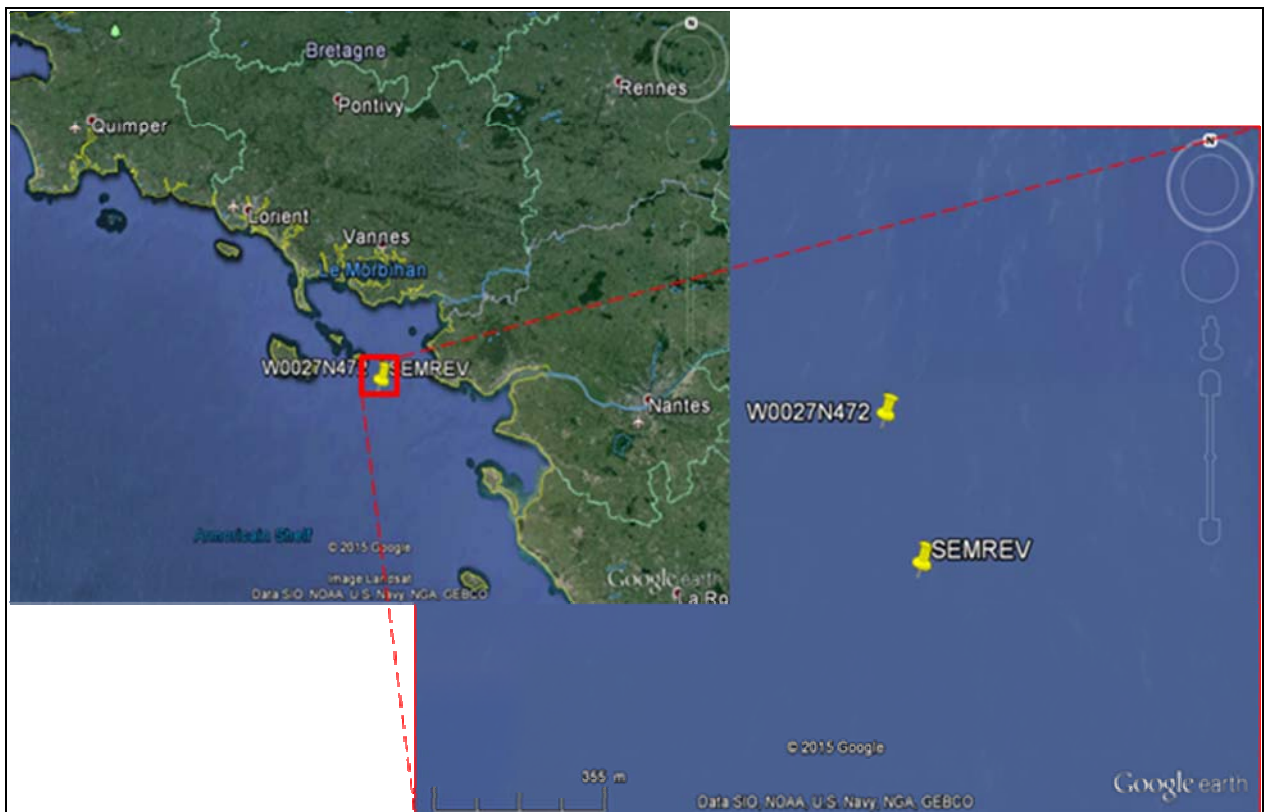


Figure 4.1: SEM-REV test site and WW3 export node W0027N472 locations.

³ <http://www.semrev.fr/fr/presentation>

4.1 IG events

The original strong IG event of interest for this study was identified prior to have happened on 06/01/2014. At the beginning of this study only WW3-IG calculations for 2008 and 2013 were available. The WW3-IG calculations for 01/2014 were conducted in summer 2015. The calculations for 2014 and 2015 use the same global grid and wind data bases and are both compared at the W0027N472 export node. Figure 4.2 and Figure 4.3 show the significant wave height H_s and the infragravity wave height H_{IG} for the grid node at 3° W - 47° N for 12/2013 and 01/2014 respectively. The presented results are the wave heights integrated over directions for the entire month with a time interval of three hours. The biggest free IG event in 12/2013 occurred on the 24/12/2013 between 06.00 h and 9.00 h (time interval: 187). For 01/2014 the biggest IG event occurs on the 07/01/2014 between 00.00 h and 03.00 h (time interval: 49).

Though the significant wave height H_s for both events is similar, the IG wave height H_{IG} on the 07/01/2014 is almost twice the H_{IG} of the 24/12/2013. The grid point at 3° W - 47° N is located about 31 km distance from the export node W0027N472.

The two identified strong IG events correspond to the following directional wave spectra (as obtained with WW3, post-processing) shown in Figure 4.4 and Figure 4.5. These spectra consist of 36 directions (360°) and 56 frequencies (f [Hz]: 0.0031 to 0.72). Both directional wave spectra show strong storm narrow banded swells coming from the west-south-west (waves "going-to" about 290°) with little directional spreading. In the IG frequency band (zoom region in the left parts of Figure 4.4 Figure 4.5) the energy spectral density distribution over frequency and direction of the IG waves is clearly visible. The almost constant f -distribution towards zero is due to the implementation in WW3 (Rawat, 2015).

While both IG events show the expected IG wave direction coming from the local reflective coastline in the region (waves "going-to" about 130°), though with a big directional spread, both events also show a second source of IG waves. This directionally narrow source with waves "going-to" about 320° , is suspected to indicate possible free IG waves coming from the Spanish north coast.

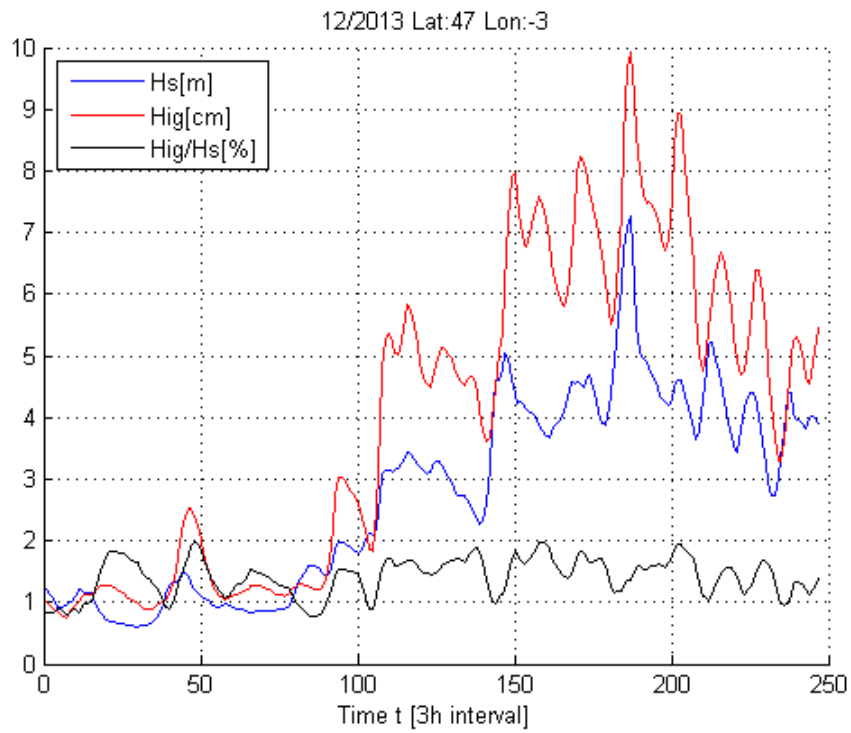


Figure 4.2: Significant wave height H_s [m] vs. H_{IG} [cm], 12/2013.

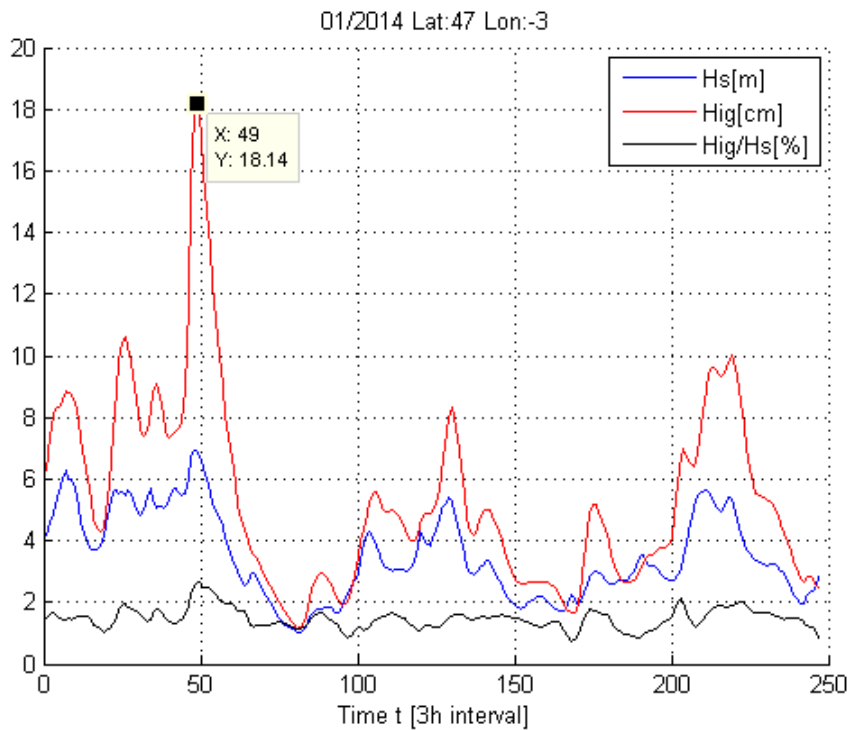


Figure 4.3: Significant wave height H_s [m] vs. H_{IG} [cm], 01/2014.

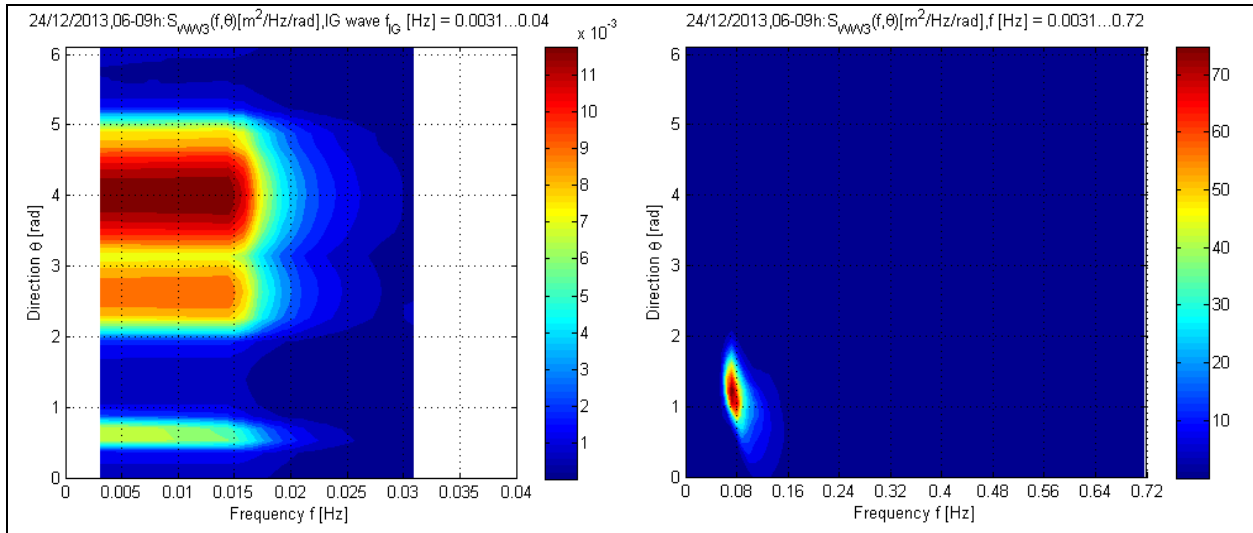


Figure 4.4: WW3-IG directional wave spectrum $S(f)$, for W0027N472, 24/12/2013, 06-09h. Left: Zoom for low-frequency (IG) band - Right: Full frequency range.

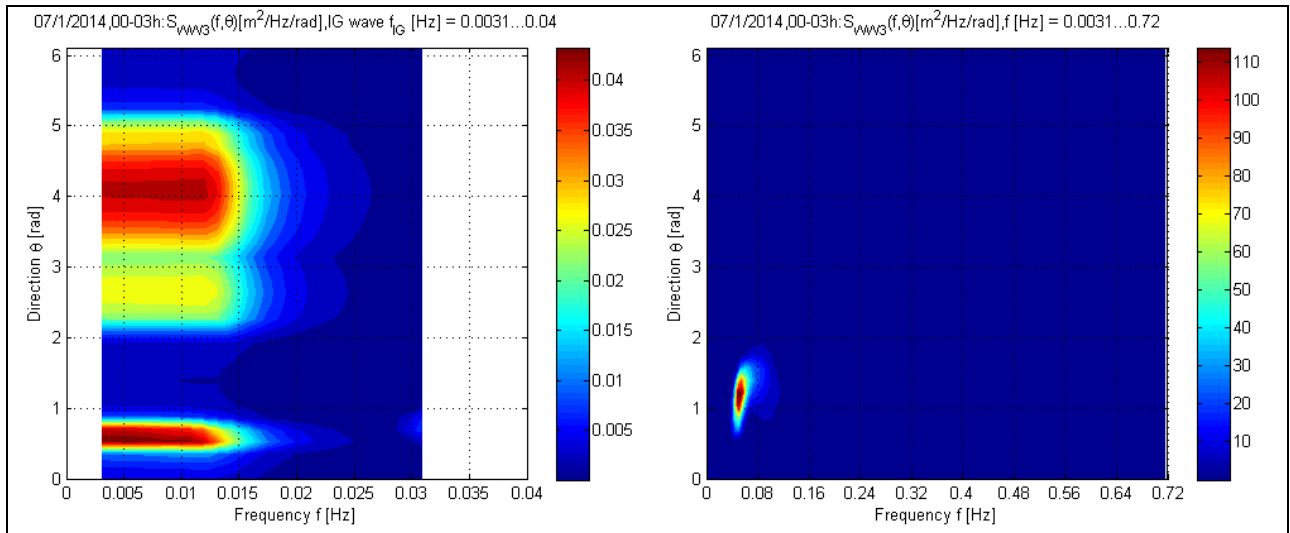


Figure 4.5: WW3-IG directional wave spectrum $S(f)$, for W0027N472, 07/01/2014, 00-03h. Left: Zoom for low-frequency (IG) band - Right: Full frequency range.

Figure 4.6 and Figure 4.7 show the 1D Amplitude spectra obtained by integrating the directional spectra over the 36 directions. In these two figures, the difference in free IG waves between the two IG events becomes clearer. Also it should be noted that for the 07/01/2014 event, due to the low peak frequency of the swell, important wave energy is found in the IG frequency range. The frequencies below 0.04 Hz are treated as free IG waves with their own wave direction (130°) and every frequency above 0.04 Hz is considered standard wave frequencies for the WF and LF calculations with the dominant swell wave direction (290°). This representation of the wave spectrum, maintaining only two wave directions, will be used in the "pseudo"-multidirectional approach.

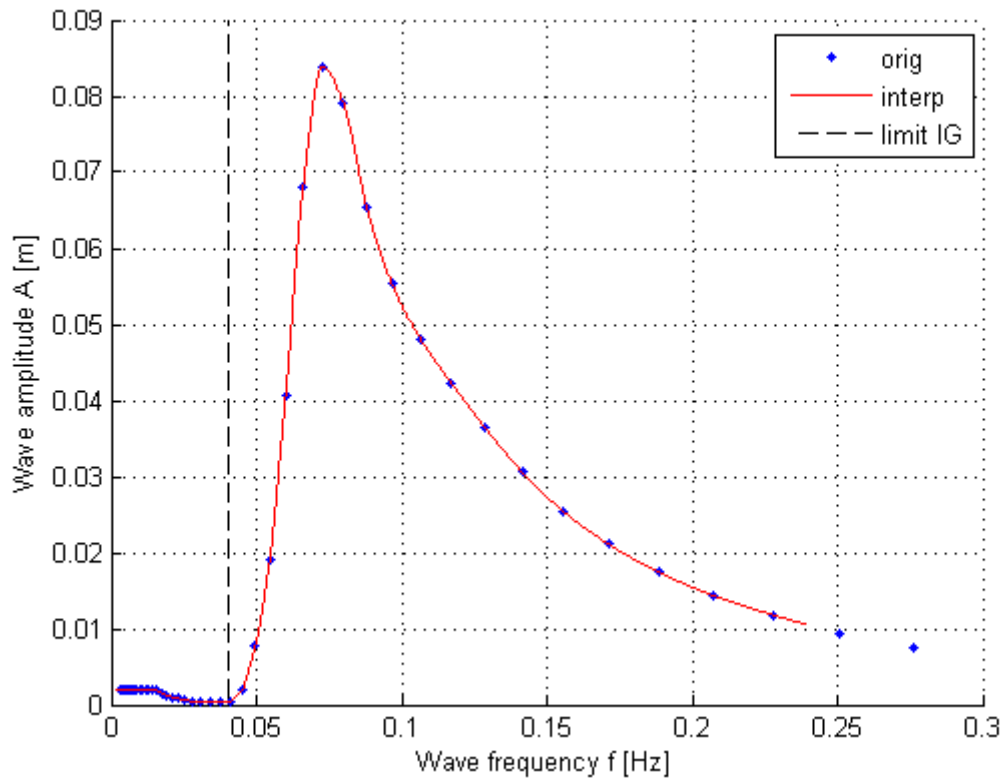


Figure 4.6: 1D Amplitude spectrum at W0027N472; 24.12.2013, 06h-09h.

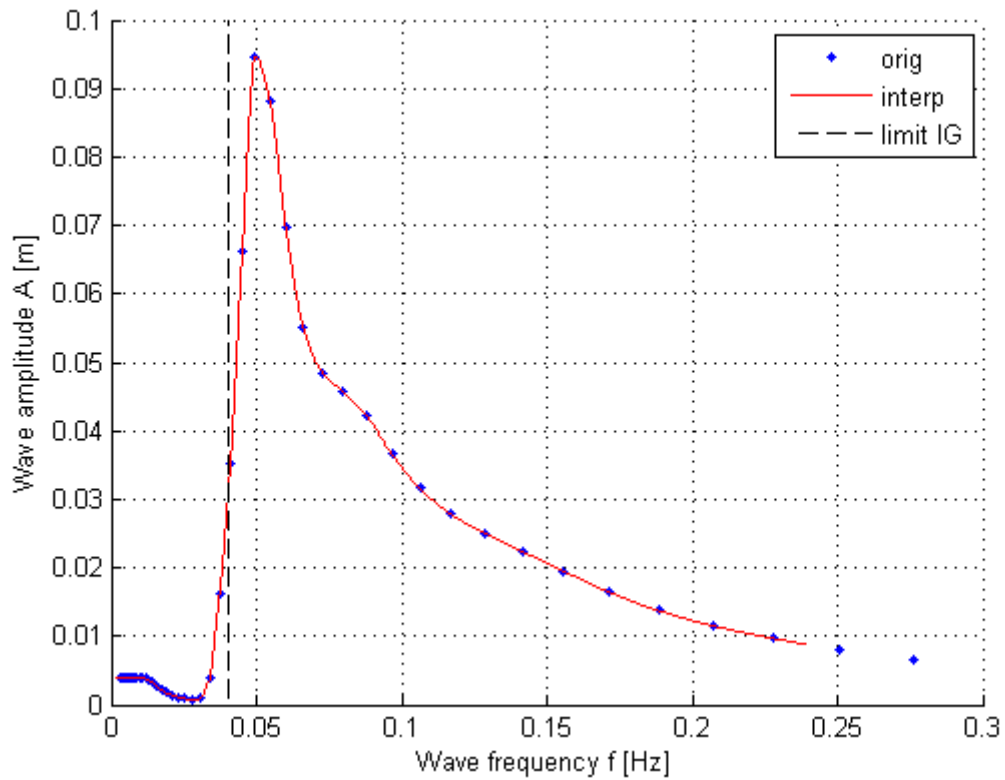


Figure 4.7: 1D Amplitude spectrum at W0027N472; 07.01.2014, 00h-03h.

4.2 Test floaters with mooring

Originally the floating structure of interest for this study was a new floater design for a floating offshore wind turbine (FOWT) to be installed soon at SEM-REV for testing. Due to unavailability of sufficient data during the project, two other moored structures have been investigated, as substitutes. The first structure is a floating storage and regasification unit (FSRU) and the second one represents a floating production and offloading unit (FPSO). Both moored floaters were tested with the two selected free IG events.

4.2.1 FSRU

The tested FSRU was originally part of the SALT2-JIP project, with physical model tests conducted at the wave basin Ifremer-Brest. The XZ- and YZ-plane symmetrical barge has the general characteristics as shown in Table 4.1. Its geometry and the mesh representation in Hydrostar are given in Figure 4.8, with the "Red" arrows representing the spread mooring, modeled as 4 horizontal springs at 45°.

Dimensions:

Length	[m]:	250
Width	[m]:	41
Draft	[m]:	18
Bilge Radius	[m]:	3.7

Mass-CoG-Inertia:

Mass	[kg]:	187000000
CoG X	[m]:	0
CoG Y	[m]:	0
CoG Z	[m]:	15
Ixx	[kgm ²]:	4.093E+10
Iyy	[kgm ²]:	7.65E+11
Izz	[kgm ²]:	7.75E+11

Mooring Stiffness:

surge	[N/m]:	1000000
sway	[N/m]:	1000000

Table 4.1: FSRU; General characteristics.

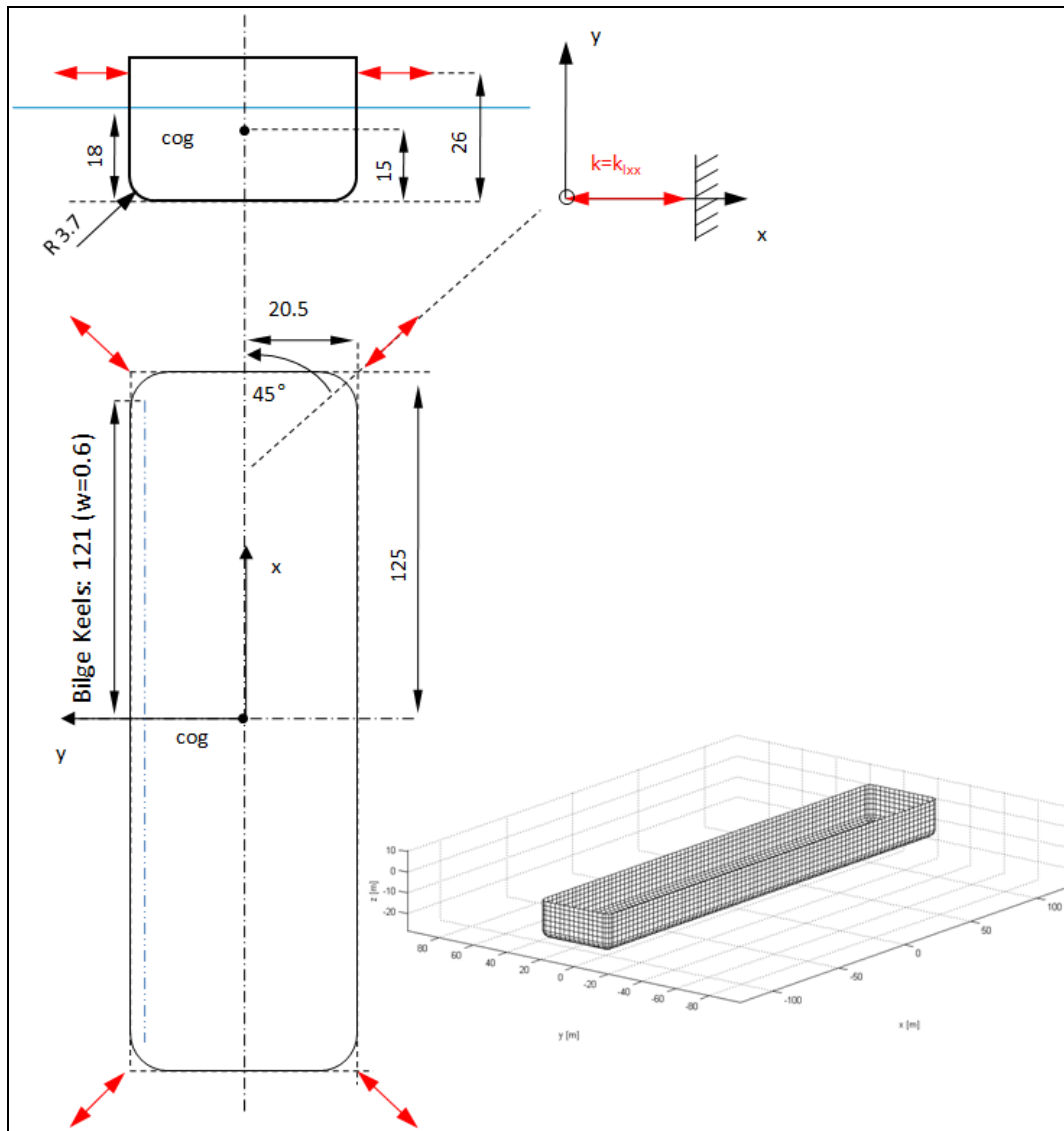


Figure 4.8: FSRU; geometry and mesh.

The additional low-frequency damping was obtained in model tests (geometric scale 1:100). The final additional damping values as input for the Hydrostar calculations were set as given in Table 4.2. Table 4.3, Table 4.4 and Table 4.5 show the Mass-Inertia Matrix, Stiffness Matrix (mooring) and Hydrostatic-Stiffness Matrix, respectively.

DAMPING_MATRIX TYPE 2 BODY 1

1 1	7.5 %
2 2	9.0 %
4 4	3.5 %
5 5	7.0 %
6 6	6.0 %

QDAMPING_MATRIX TYPE 1 BODY 1

4 4	4.7652E+10
-----	------------

Table 4.2: FSRU; Additional damping (input for Hydrostar).

Mass-Inertia:

187000000	0	0	0	0	0
0	187000000	0	0	0	0
0	0	187000000	0	0	0
0	0	0	4.093E+10	0	0
0	0	0	0	7.6486E+11	0
0	0	0	0	0	7.7466E+11

Table 4.3: FSRU; Mass-Inertia Matrix for Hydrostar.

Stiffness (Mooring):

1.0293E+06	0	0	0	1.1323E+07	0
0	1.0293E+06	0	-1.1323E+07	0	0
0	0	5.8651E+04	0	0	0
0	-1.1323E+07	0	1.4920E+08	0	0
1.1323E+07	0	0	0	1.0410E+09	0
0	0	0	0	0	1.1541E+10

Table 4.4: FSRU; Stiffness-Matrix (Mooring).

Hydrostatic Stiffness:

0	0	0	0	0	0
0	0	0	0	0	0
0	0	0.1029E+09	0	0	0
0	0	0	0.3472E+10	0	0
0	0	0	0	0.5239E+12	0
0	0	0	0	0	0

Table 4.5: FSRU; Hydrostatic Stiffness.

4.2.2 FPSO

The second floating structure in this study is a FPSO, which was used for the CITEPH-CHEEPP2 project (Prevosto, 2010; MLKF2 structure "BUMI - Armada Perkasa", see Figure 4.9). In comparison to the FSRU, the mesh file for the geometry of this floater was already available. The mooring system is a spread mooring (see Figure 4.10, right). The final mesh with the applied draft (see Table 4.6) is shown in Figure 4.11.



Figure 4.9: FPSO; BUMI - Armada Perkasa.

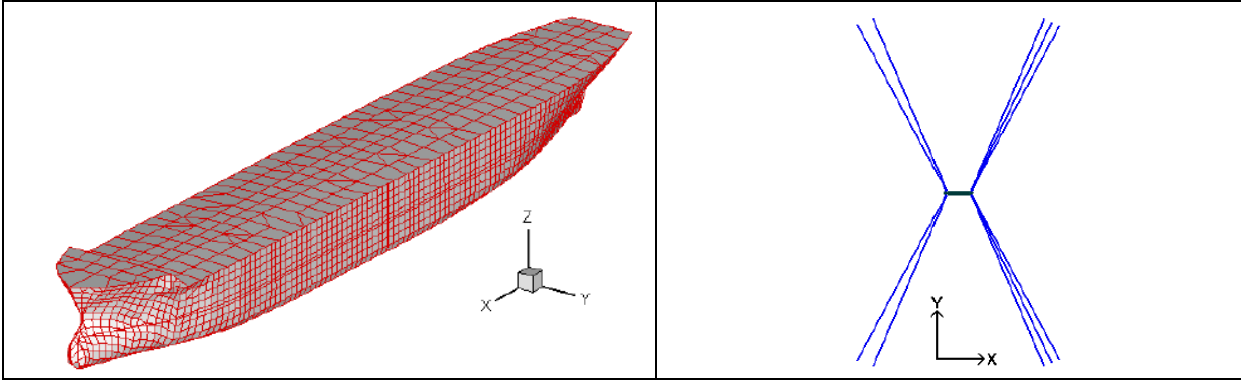


Figure 4.10: FPSO; Left: Mesh - Right: Mooring configuration.

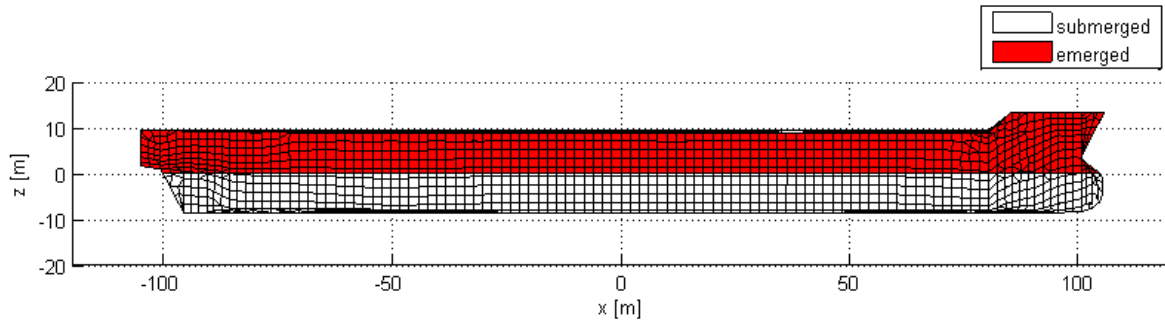


Figure 4.11: FPSO; Geometry with draft applied.

Dimensions:

Length	[m]:	221.2
Width	[m]:	32.2
Draft	[m]:	8.64

Characteristics:

Mass	[kg]:	4.4976E+07
CoG X	[m]:	5.67
CoG Y	[m]:	0
CoG Z	[m]:	1.34

Mooring Stiffness:

surge	[N/m]:	6.8390E+04
sway	[N/m]:	2.9610E+05

Table 4.6: FPSO; General characteristics.

In order to use this FPSO structure for the present study, the original results from the CITEPH-CHEEPP2 project for motion- and force-RAO, as well as the QTF, obtained with DIODORE were tried to be reproduced. This process involved overcoming some inconsistencies in the original data set and is further documented in Appendix A.

The final values for mass-inertia, mooring-stiffness and hydrostatic stiffness and additional damping are shown in Table 4.7, Table 4.8, Table 4.9 and Table 4.10, respectively.

Mass-Inertia:

44976000	0	0	0	0	0
0	44976000	0	0	0	0
0	0	44976000	0	0	0
0	0	0	2,76E+09	0	0
0	0	0	0	1,23E+11	0
0	0	0	0	0	1,24E+11

Table 4.7: FPSO; Mass-Inertia matrix.

Stiffness (Mooring):

68390	-0,0039	1848	0	5728000	0
-0,0039	296100	0,001	-4436000	0	-5233000
1748	0	63250	0,0156	-411400	0,25
-0,0312	-4334000	0	70400000	2	18140000
5414000	-0,125	-418200	4	621800000	-8
0	-5233000	-0,125	19650000	32	2,14E+09

Table 4.8: FPSO; Stiffness (Mooring) matrix.

Hydrostatic Stiffness:

0	0	0	0	0	0
0	0	0	0	0	0
0	0	5,37E+07	0	1,04E+08	0
0	0	0	1,10E+10	0	0
0	0	1,04E+08	0	1,39E+11	0
0	0	0	0	0	0

Table 4.9: FPSO; Hydrostatic stiffness matrix.

DAMPING_MATRIX TYPE 1 BODY 1

1 1	4.36E+05
2 2	1.37E+05
6 6	9.66E+09

QDAMPING_MATRIX TYPE 1 BODY 1

4 4	4.62E+09
-----	----------

Table 4.10: FPSO; Additional damping (input for Hydrostar).

5 Results

To evaluate the importance of the effect of free IG waves to moored floating structures, the wave forces and the motion response due to these exciting forces have to be compared for the WF, LF and IG frequency range. The water depth for the HYDROSTAR calculations was set to $h = 40$ m.

5.1 Mechanical transfer function

As shown in Figure 3.1, the motion response is obtained by using the wave forces together with an inverse, linear second order transfer function, which includes mass, inertia, damping and stiffness, describing the mechanical floater-mooring system. The same mechanical transfer function (MTF) is used to obtain the motion response for the WF forces, LF forces and free IG forces. Figure 5.1 and Figure 5.2 show the modulus of H_x^{-1} for the FSRU and the FPSO, respectively.

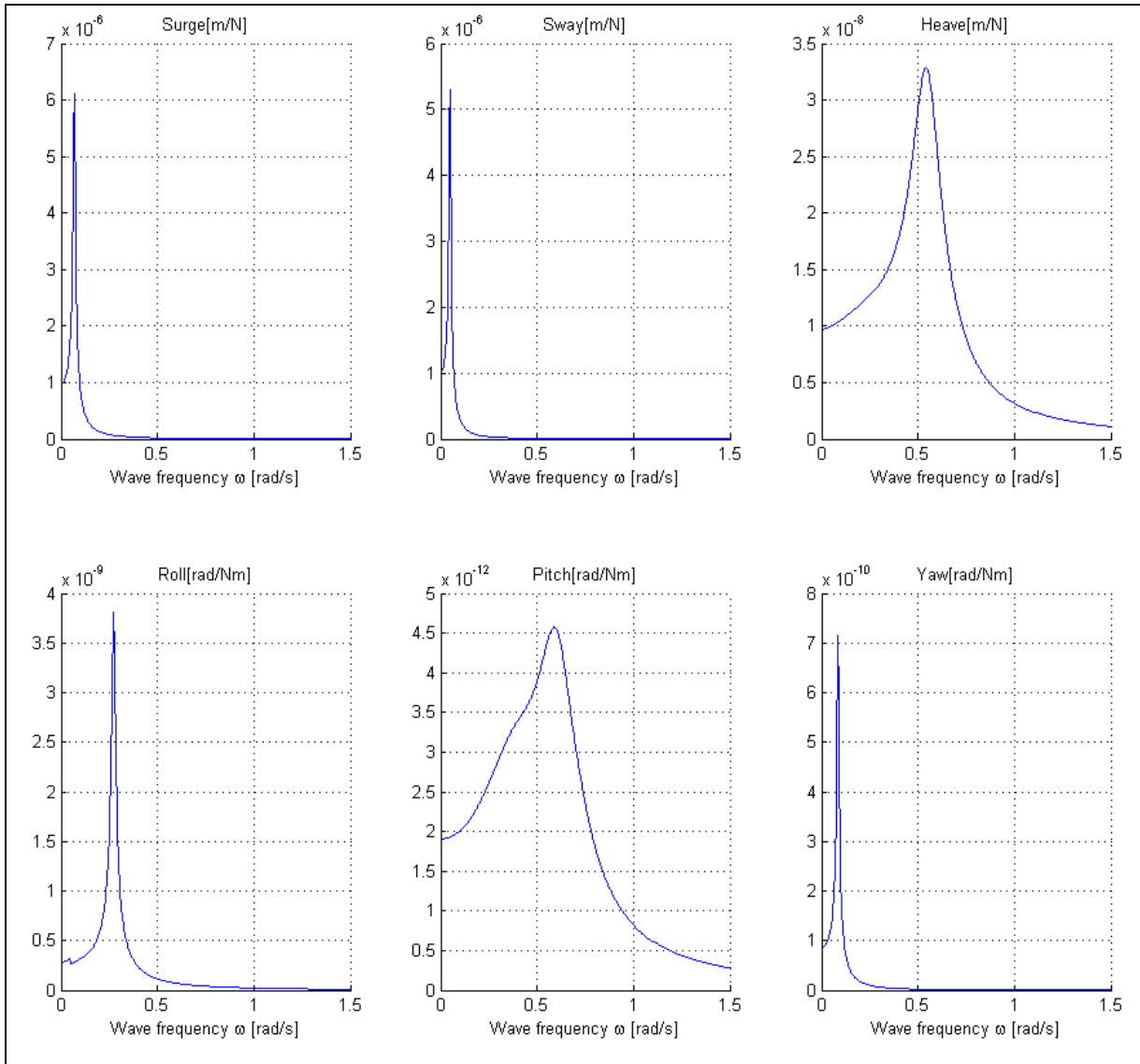


Figure 5.1: FSRU; Mechanical transfer function (modulus).

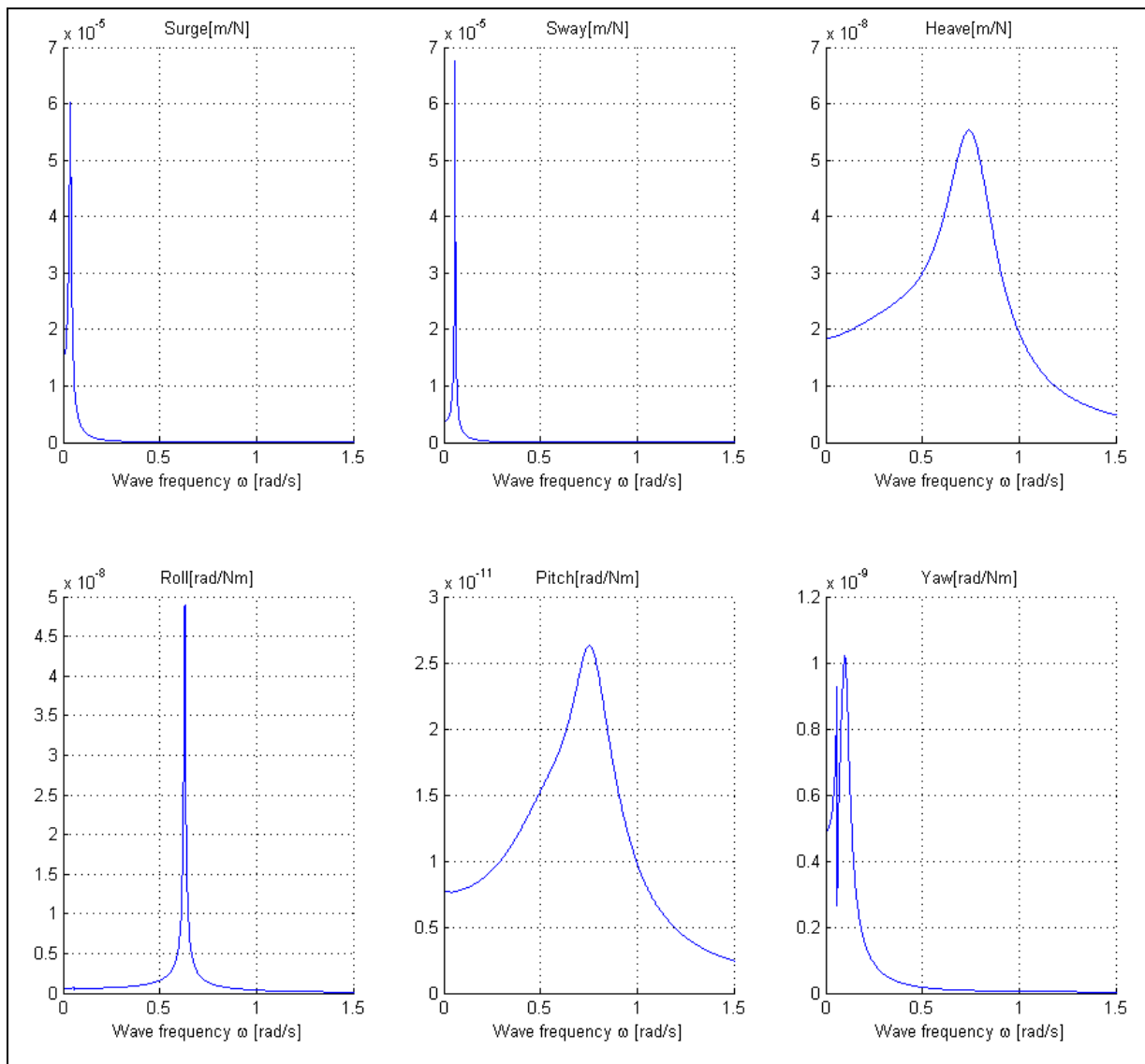


Figure 5.2: FPSO; Mechanical transfer function (modulus).

With a free IG frequency limit of $f_{lim IG}$ [Hz]= 0.04 and $\omega_{lim IG}$ [rad/s] \approx 0.25, it can be clearly seen that the resonant frequencies of both structures ,FSRU and FPSO, in *Surge*, *Sway* and *Yaw* are well within the free IG frequency range. Since the MTF is the same for both, the calculation of the LF motion response and the calculation for the free IG motion response, the difference in the low-frequency motion response is only a result of the difference between LF and free IG wave exciting forces.

5.2 Motion LTF (Motion RAOs)

The linear transfer function for the motion response of the moored floaters, the response amplitude operator (RAO) combines the mechanical transfer function and the linear transfer function for the first order wave forces. Since the wave exciting forces vary for different incidence angles between waves and structure, the motion RAOs modulus shown in Figure 5.3 and Figure 5.4, as obtained with HYDROSTAR, are presented for incidence angles between 0° and 180° . For both (ship) floaters the maximum motion response for translation occurs for beam seas, which is the case in our study considering a standard orientation of the floater of 0° (bow facing North) and the two selected free IG events with dominant wave directions being $\approx 290^\circ$ (swell) and $\approx 130^\circ$ (free IG waves).

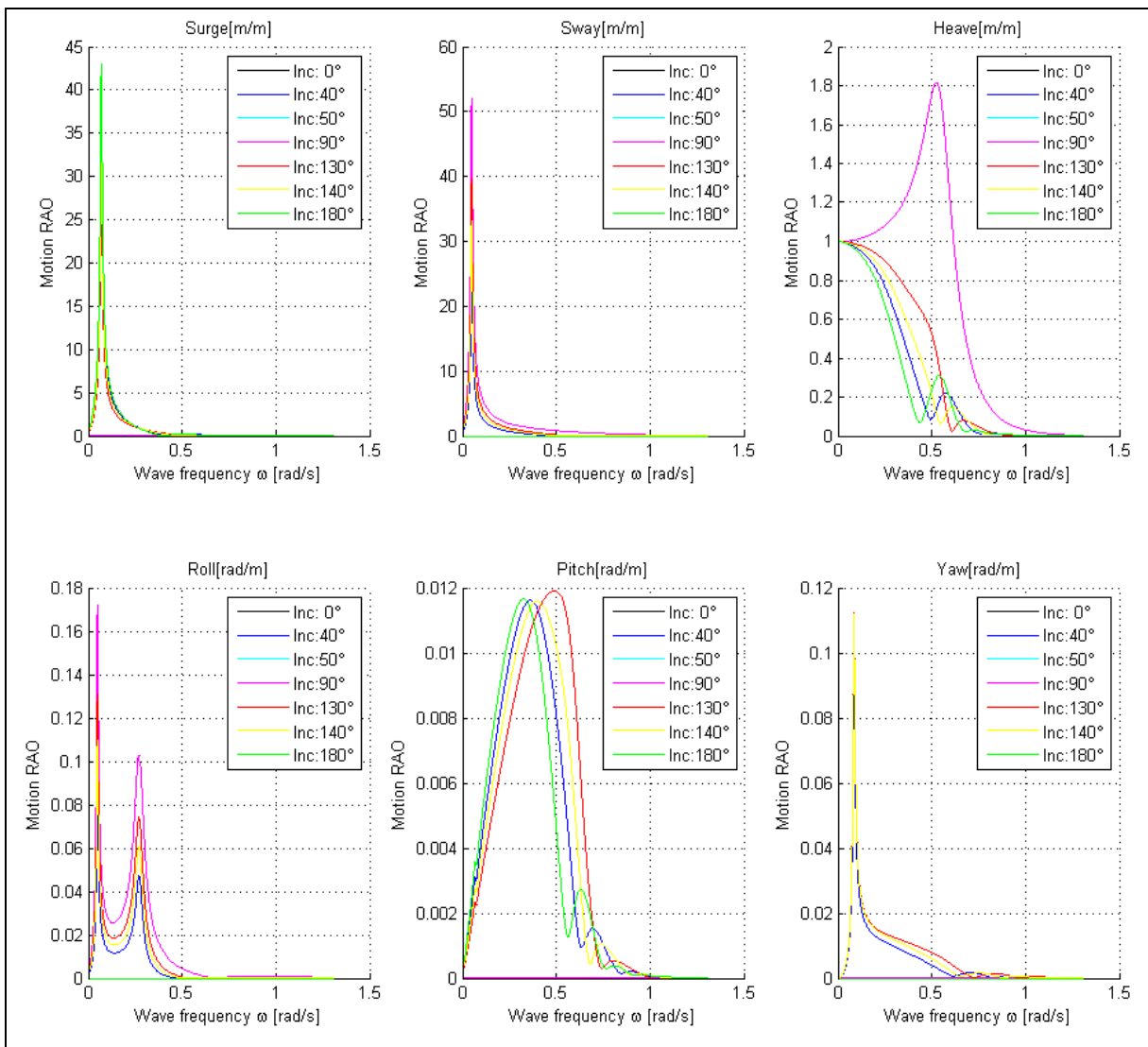


Figure 5.3: FSRU; Motion RAOs (modulus) for different wave incidence directions.

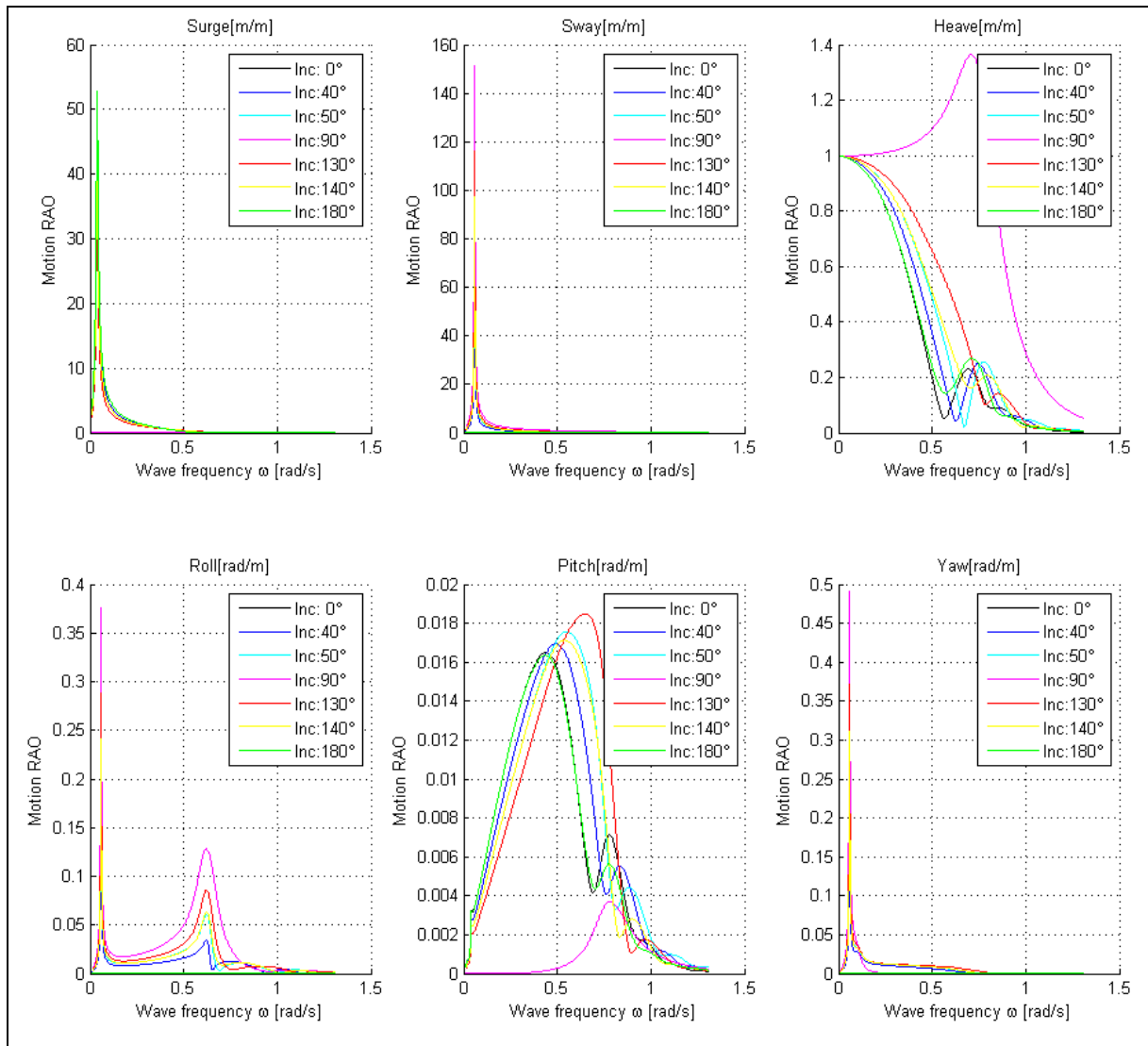


Figure 5.4: FPSO; Motion RAOs (modulus) for different wave incidence directions.

The motion response for WF and free IG frequencies is obtained by multiplication of the motion-RAOS with the Fourier coefficients of the free surface elevation (wave spectrum times normal distributed random complex variable). The time series of the motions then is obtained by inverse Fourier transformation of the first order motion response.

Force LTF (Force RAOs)

The linear transfer functions for force (force RAOs) together with the wave spectrum are used to obtain the force time series for WF and free IG, similar to the motion time series for WF and free IG.

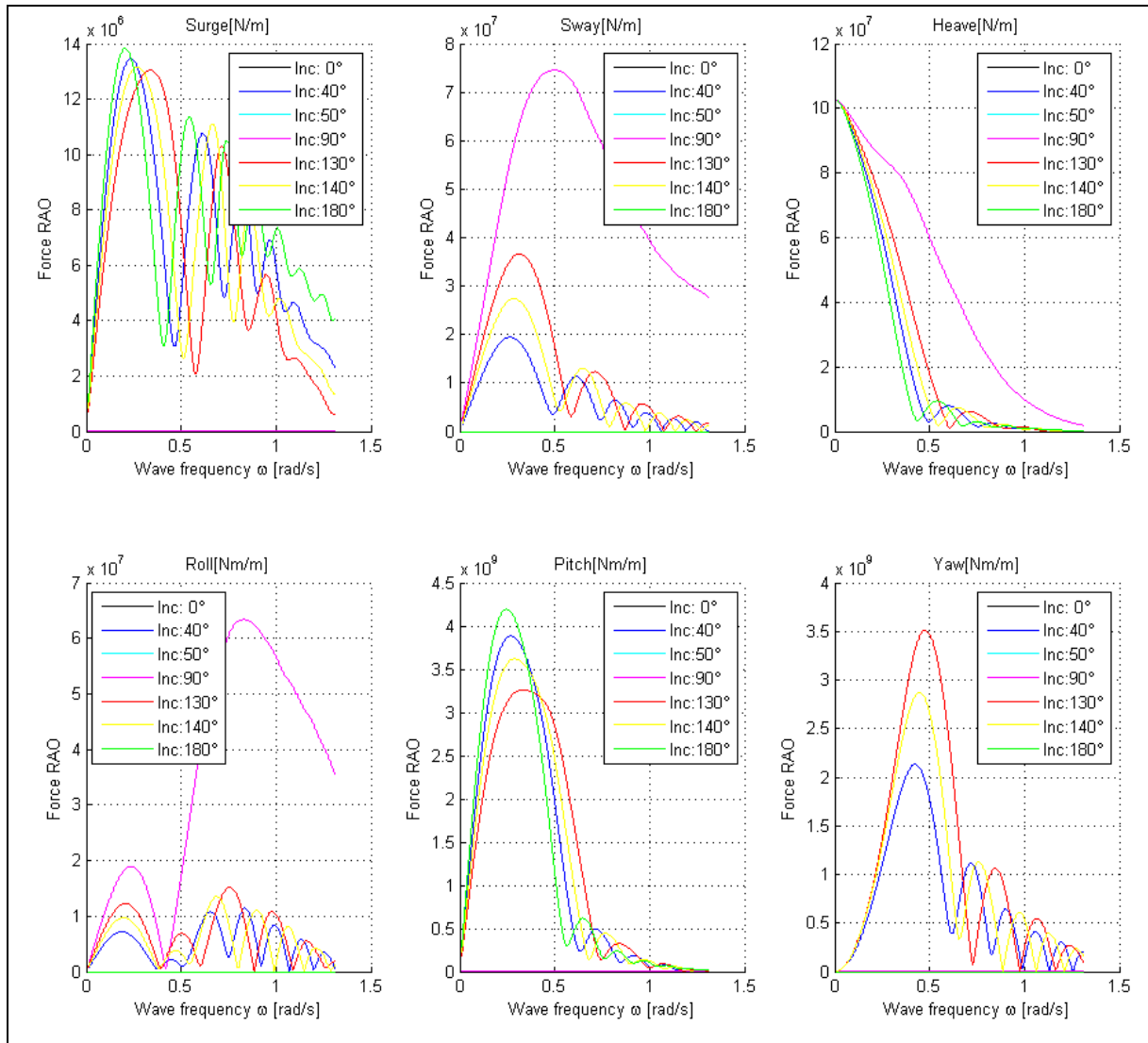


Figure 5.5: FSRU; Force RAOs (modulus) for different wave incidence directions.

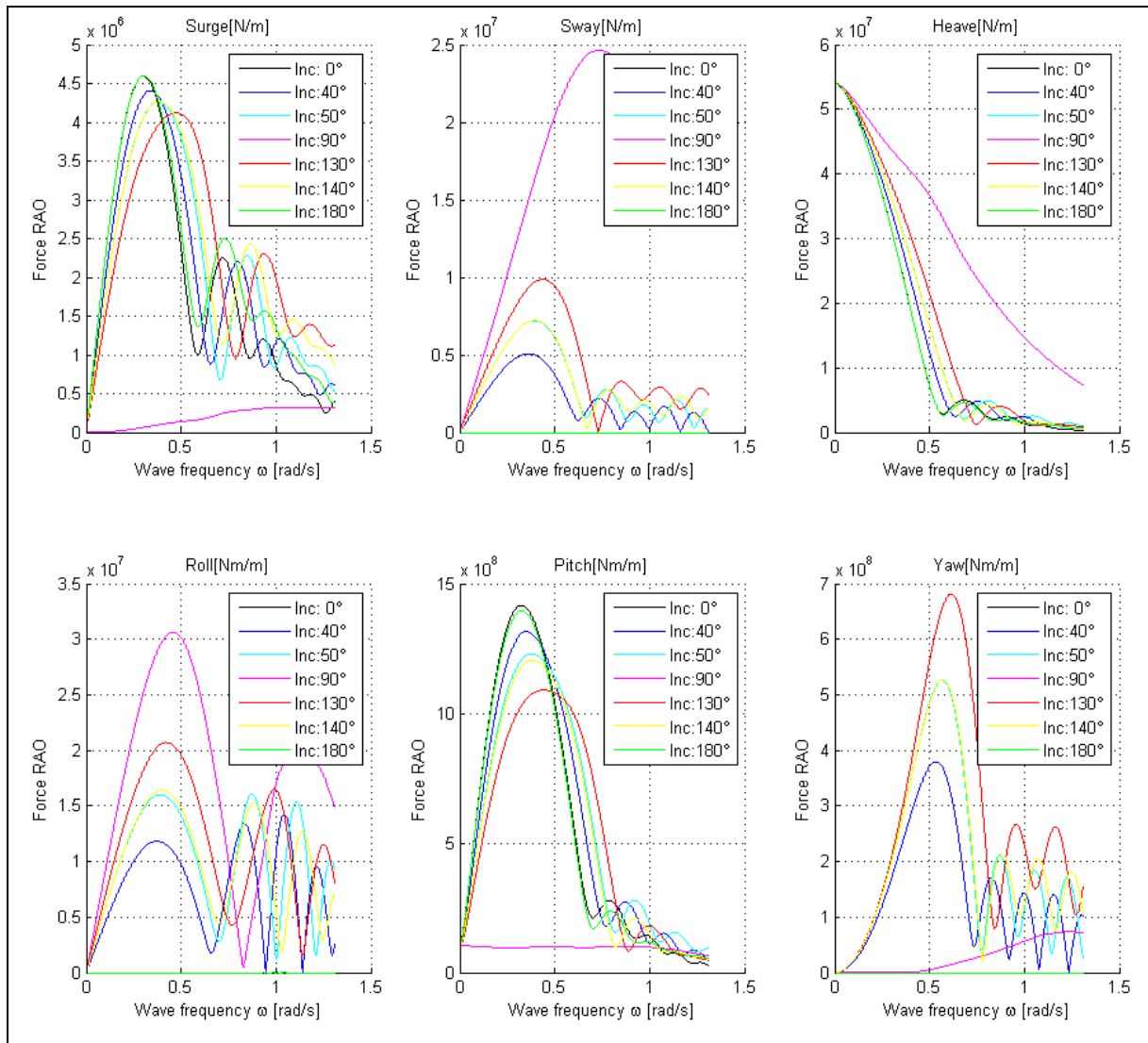


Figure 5.6: FPSO; Force RAOs (modulus) for different wave incidence directions.

5.3 Force QTF

For the "pseudo"-multidirectional approach (swell going towards 290°, free IG waves going to 130°) and standard orientation of the floater (bow facing North) the QTF are calculated with a wave incidence resolution of 10° (0°-350°). Figure 5.7 and Figure 5.8 show the QTFs for uni-directional waves (wave incidence: 290°) for the FSRU and the FPSO floater, respectively. Each figure shows on top the moduli of the QTF, while the bottom shows the phases, for Surge, Sway and Yaw (from left to right).

The QTFs are calculated for wave frequencies between $\omega_{1,2}$ [rad/s] = 0.24...1.5 and difference frequencies $\Delta\omega$ [rad/s] = 0...0.24. Clearly visible for both, FSRU and FPSO are the high main diagonal values for the Surge and Sway QTFs, related to the steady drift forces.

For 4D-QTF there is one QTF for every possible combination of two incidence directions. The QTFs shown in Figure 5.7 and Figure 5.8 represent one 2D combination of $\beta_1 = \beta_2 = 290^\circ$.

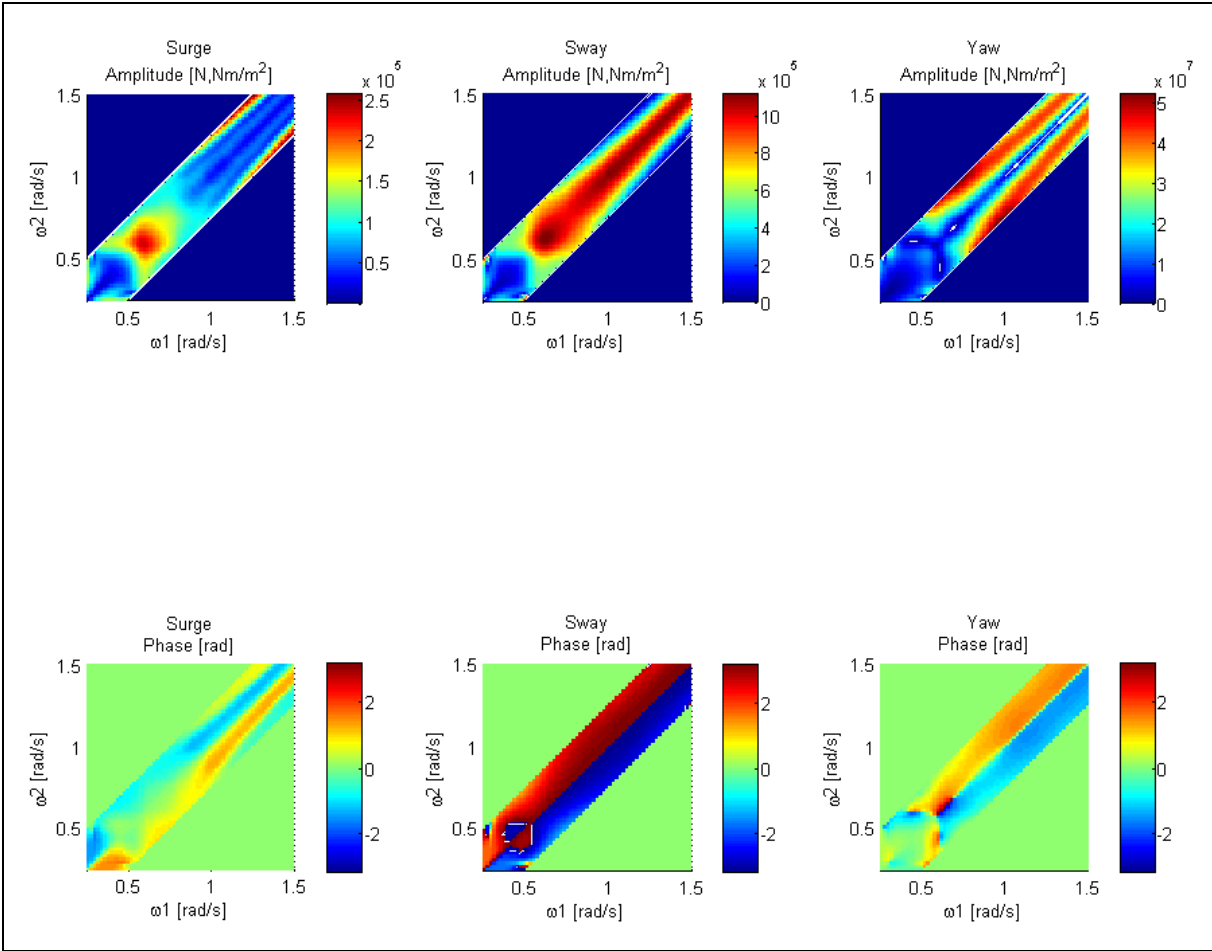


Figure 5.7: FSRU, QTF (290° wave incidence).

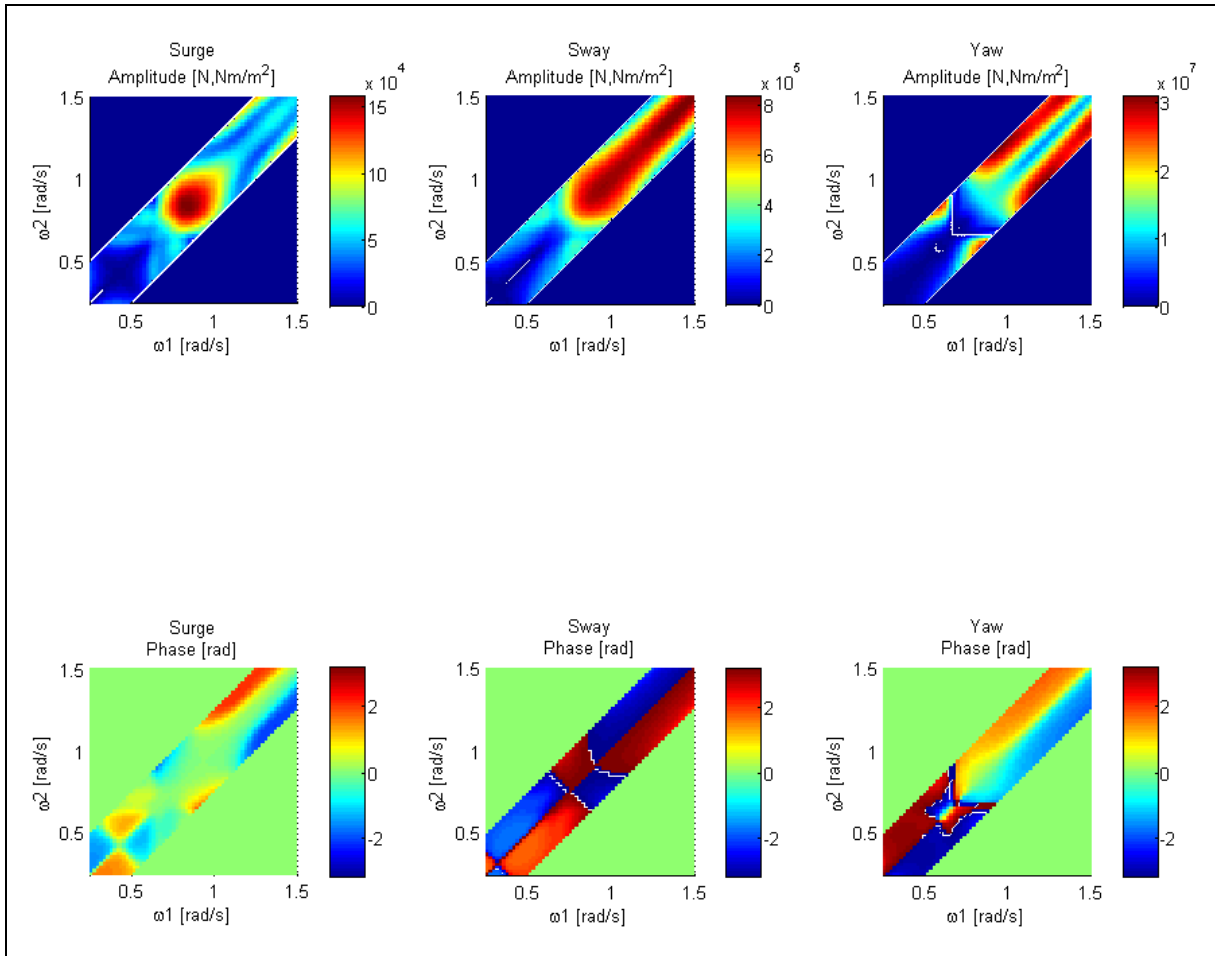


Figure 5.8: FPSO, QTF (290° wave incidence).

5.4 Low frequency wave forces

The present study aims to evaluate the influence of free IG waves on moored floating structure response. The inclusion of free IG waves represents an additional low-frequency excitation. As shown in Section 5.1, the difference between the second order LF forces and the forces due to free IG waves is a direct indication for the importance of free IG waves to the selected floater and moorings system. While the LF forces for a wave incidence of 290° , the forces due to free IG waves are for a wave incidence on 130° . In this "pseudo"-multi directional approach the total wave forces and the resulting motion responses are obtained by linear superposition of the separate results for WF, LF and IG.

The following figures show the comparison of the absolute values (moduli) of these low-frequency wave forces (second order LF and free IG) in frequency space. Superposed on this comparison is the mechanical transfer function (MTF) for each degree of freedom, in order to highlight the important frequency ranges, which are mainly important for the motion response.

Figure 5.9 and Figure 5.10 show the low-frequency force comparison (absolute values) for the FSRU. Figure 5.9 shows the results for the IG event on 24/12/2013 between 06h and 09h, while Figure 5.10 shows the results for the IG event on 07/01/2014 between 0h and 03h.

Figure 5.11 and Figure 5.12 show the low-frequency force comparison (absolute values) for the FPSO. Figure 5.11 shows the results for the IG event on 24/12/2013 between 06h and 09h, while Figure 5.12 shows the results for the IG event on 07/01/2014 between 0h and 03h.

For both selected structures, FSRU and FPSO, the second order LF forces for Surge, Sway and Yaw are bigger than the low frequency forces due to free IG waves in the important frequency ranges according to the MTFs.

The presented results in Figure 5.9 to Figure 5.12 do not include a correction of large displacements or changes in orientation (see Figure 3.1) and are obtained for a standard orientation of the floater (bow facing North).

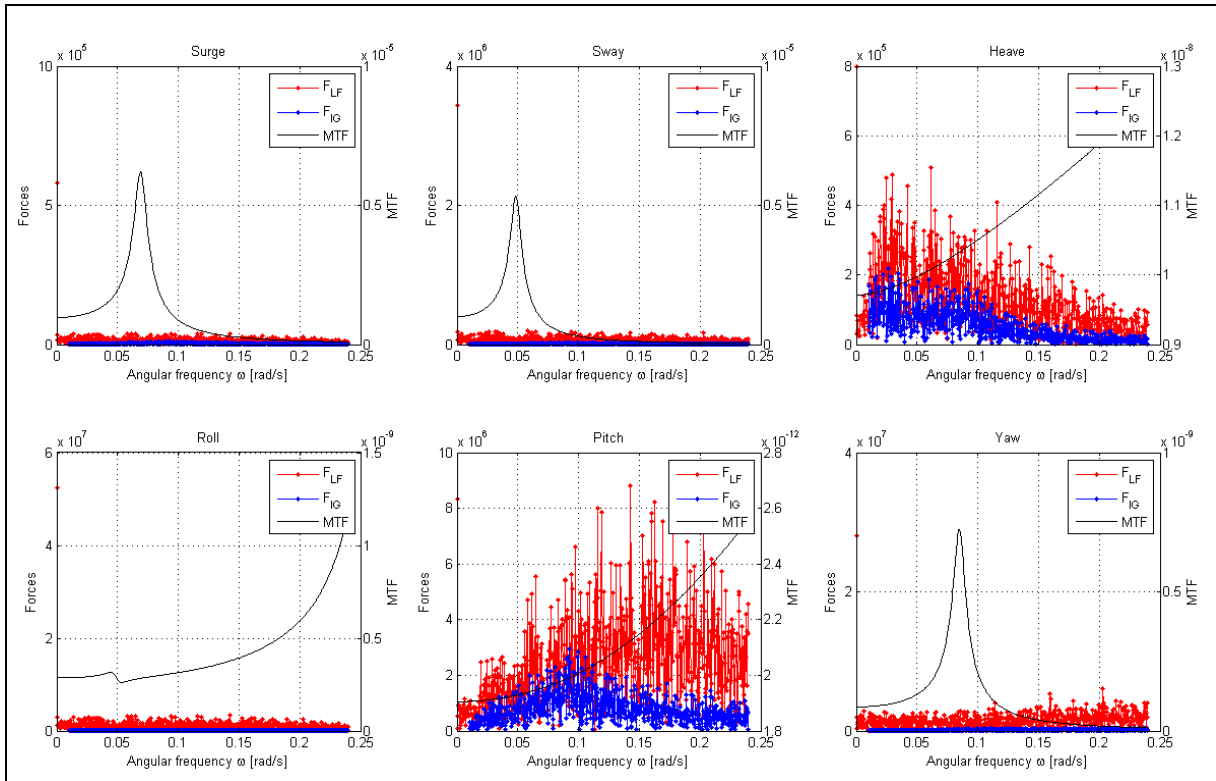


Figure 5.9: FSRU; Low frequency forces and MTF, 24/12/2013, 06h-09h.

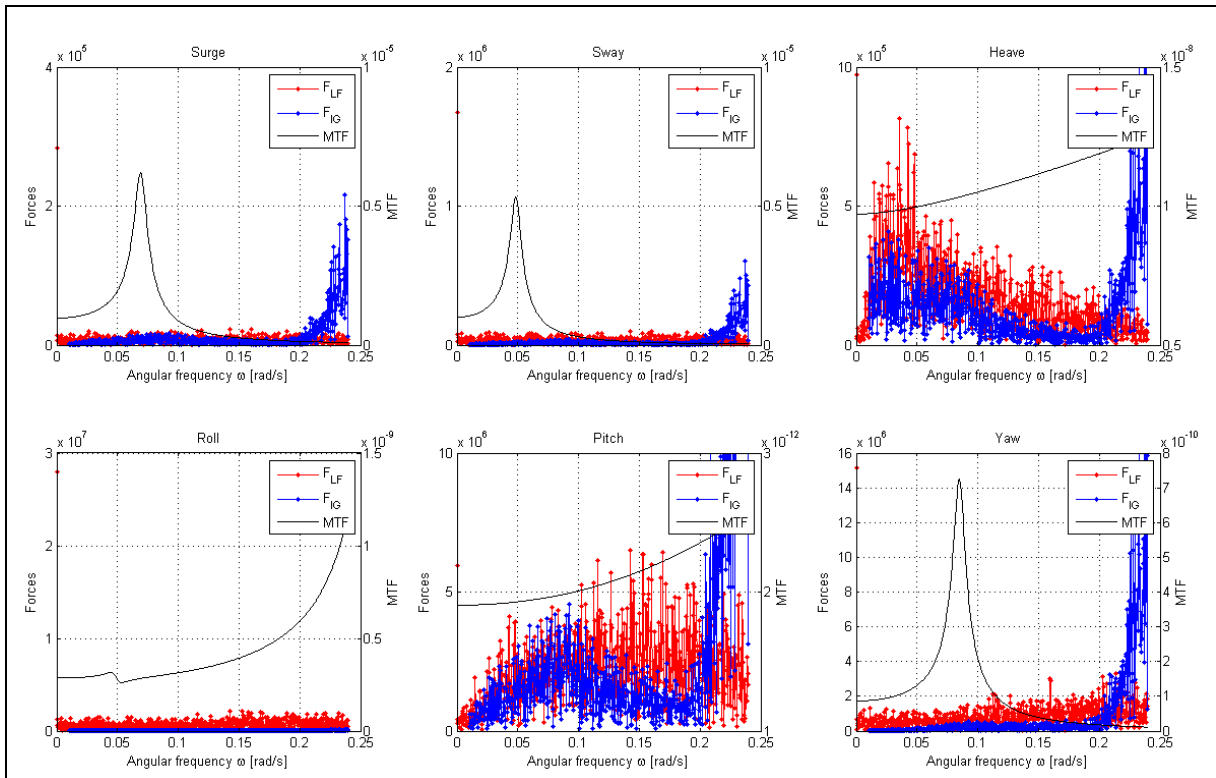


Figure 5.10: FSRU; Low frequency forces and MTF, 07/01/14, 00h-03h.

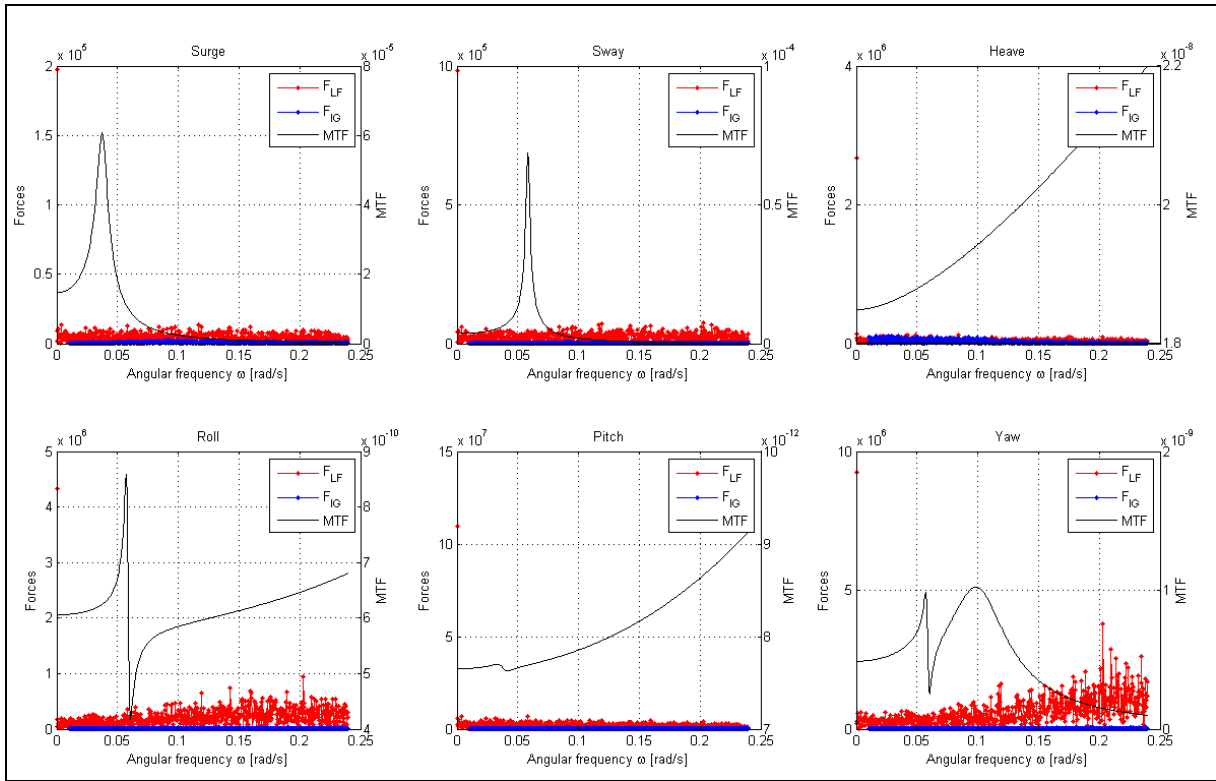


Figure 5.11: FPSO; Low frequency forces and MTF, 24/12/2013, 06h-09h.

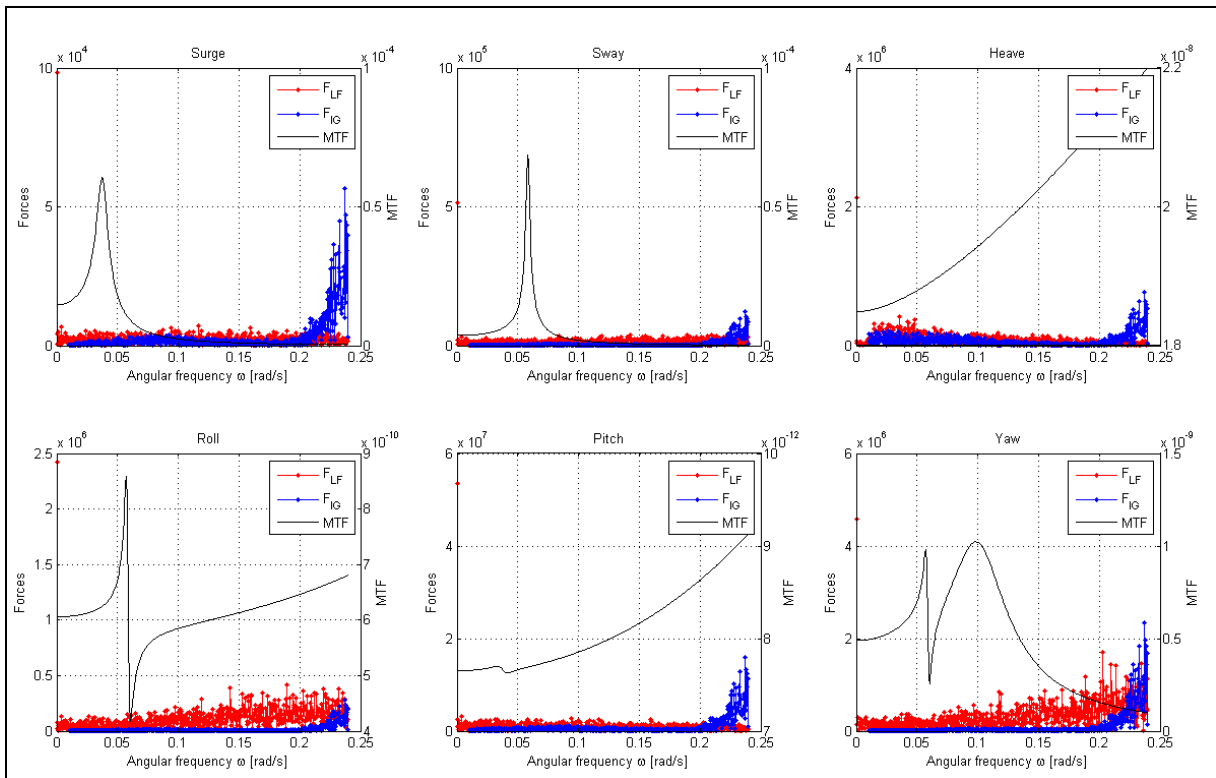


Figure 5.12: FPSO; Low frequency forces and MTF, 07/01/2014, 00h-03h.

5.5 Motion response

The motion response of the moored floater to the exciting wave frequencies is obtained by applying the mechanical transfer function (MTF). Again, since the same MTF is used for all exciting wave forces, the importance of free IG waves becomes clearest by comparing the low-frequency range ($\omega[\text{rad/s}] = 0 \dots 0.25$) for the resulting motions.

Similar to the low frequency forces, Figure 5.13 and Figure 5.14 show the low frequency motions separately in frequency space (absolute values) for the FSRU. Figure 5.13 showing the results for the IG event on 24/12/2013 between 06h and 09h, while Figure 5.14 shows the results for the IG event on 07/01/2014 between 0h and 03h.

Figure 5.15 and Figure 5.16 show the low-frequency force comparison (absolute values) for the FPSO. Figure 5.15 shows the results for the IG event on 24/12/2013 between 06h and 09h, while Figure 5.16 shows the results for the IG event on 07/01/2014 between 0h and 03h.

As expected from the low frequency forces, the motions as a result to second order LF forces are bigger than the motions as result to free IG waves.

As the total motions of the moored floaters have been considered in this first analysis as the superposition of the motions due to WF, LF and free IG, the total values of the reconstructed time series of motion for each degree of freedom have to be compared.

In order to evaluate the importance of free IG, the RMS values of a reconstructed 3h time series for the total motions are compared for

- a) LF (LF)
- b) LF + free IG (LFIG)
- c) WF + LF (GWLF)
- d) WF + LF + free IG (GWLFIG)

The results for the RMS values for all degrees of freedom are presented in Figure 5.17 and Figure 5.18.

Again, the presented results do not include a correction of large displacements or changes in orientation (see Figure 3.1) and are obtained for a standard orientation of the floater (bow facing North).

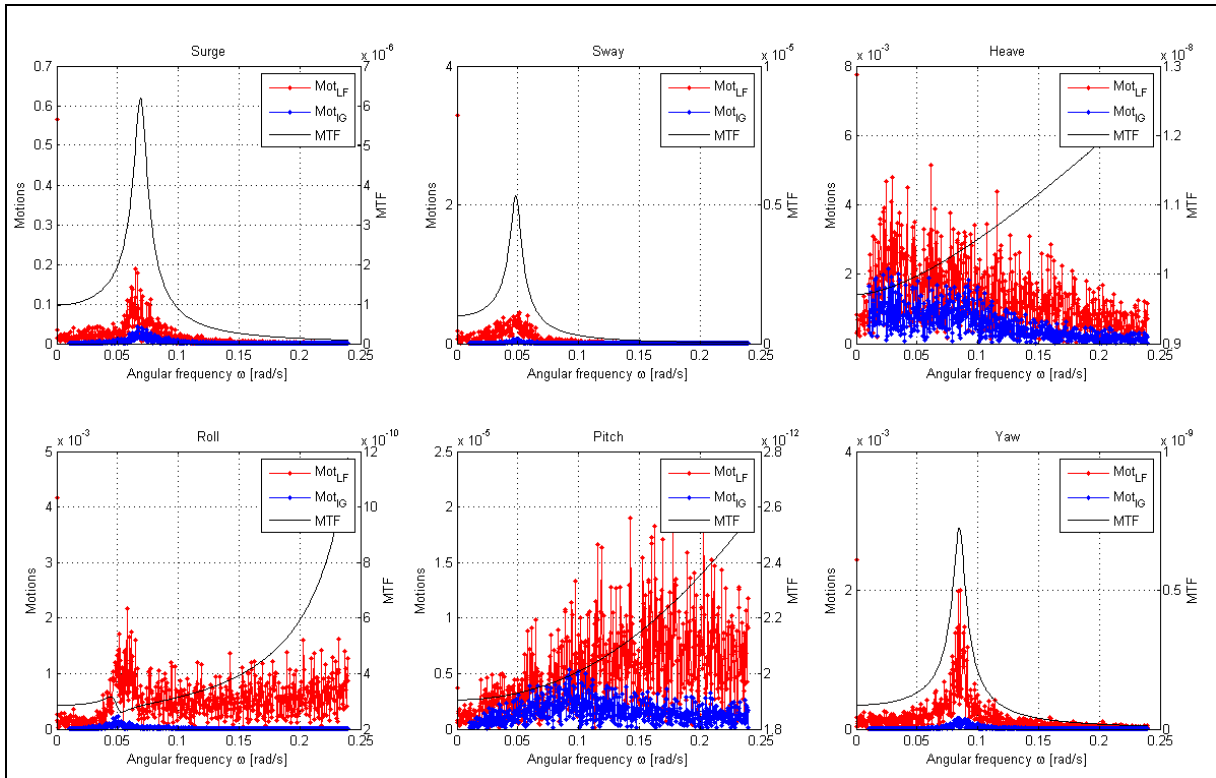


Figure 5.13: FSRU; Low frequency motions and MTF, 24/12/2013, 06h-09h.

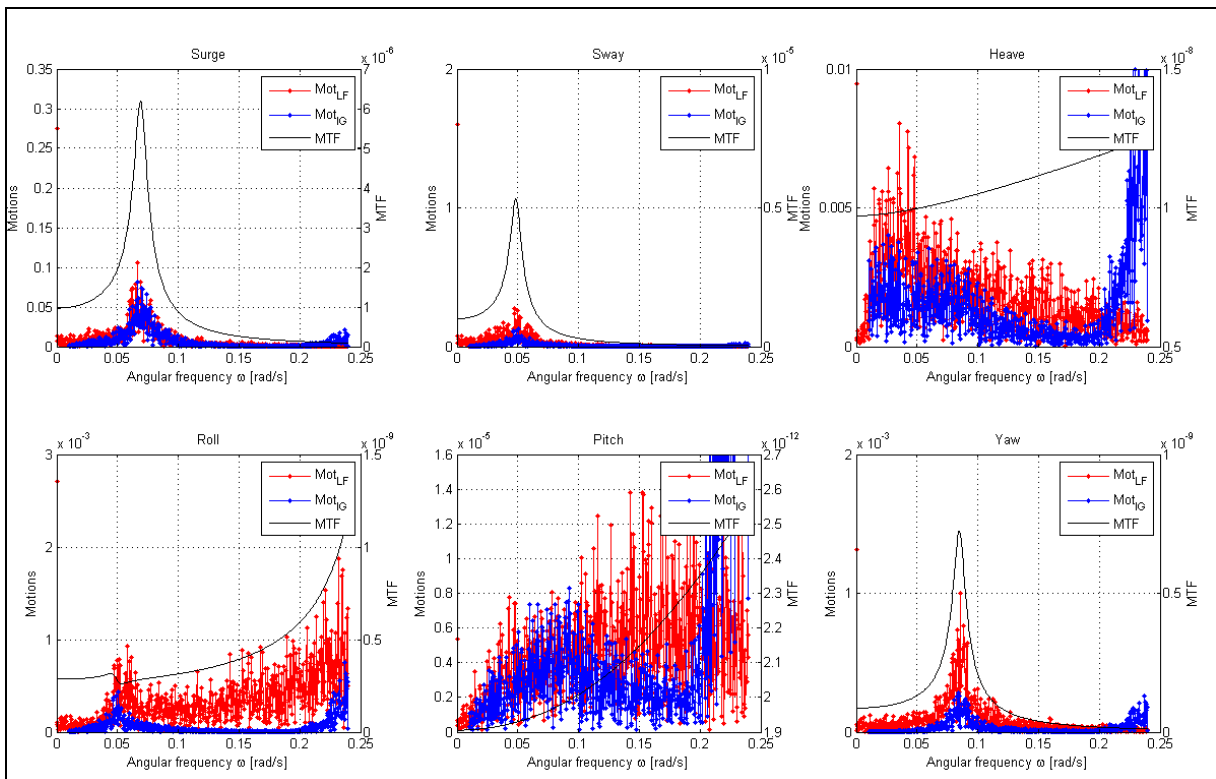


Figure 5.14: FSRU; Low frequency motions and MTF, 07/01/2014, 00h-03h.

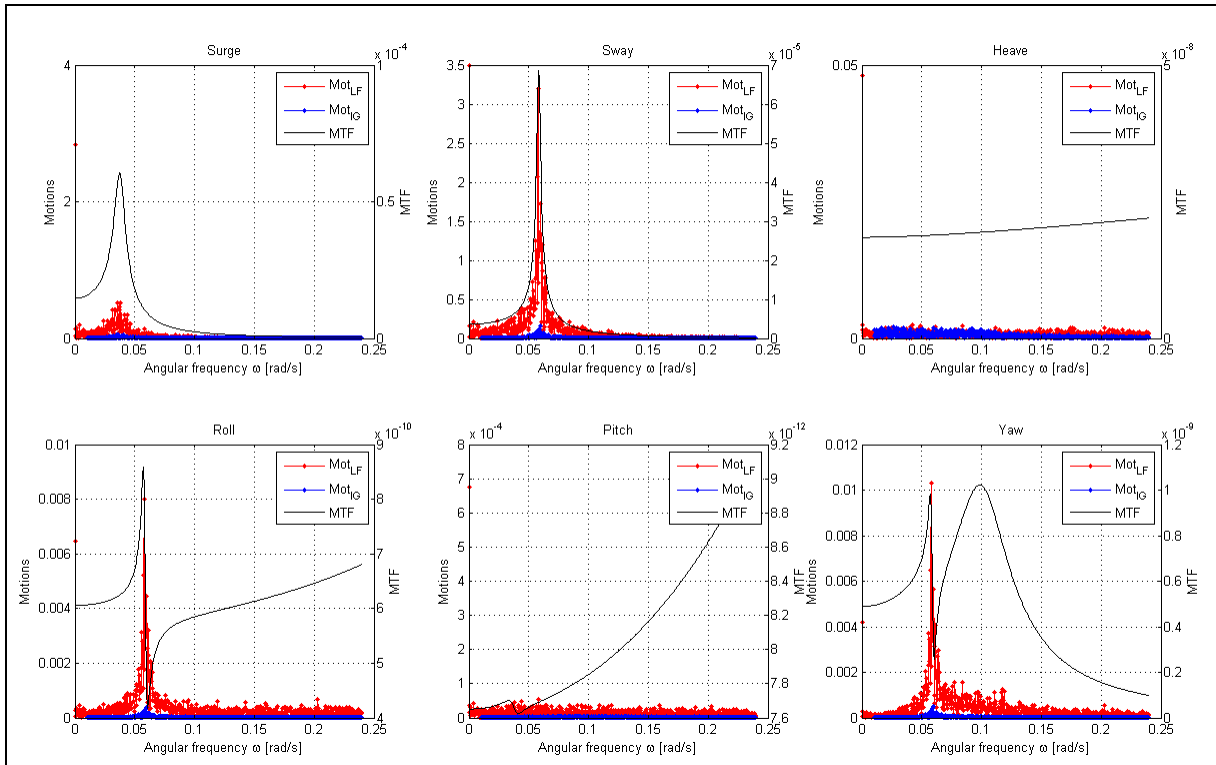


Figure 5.15: FPSO; Low frequency motions and MTF, 24/12/2013, 06h-09h.

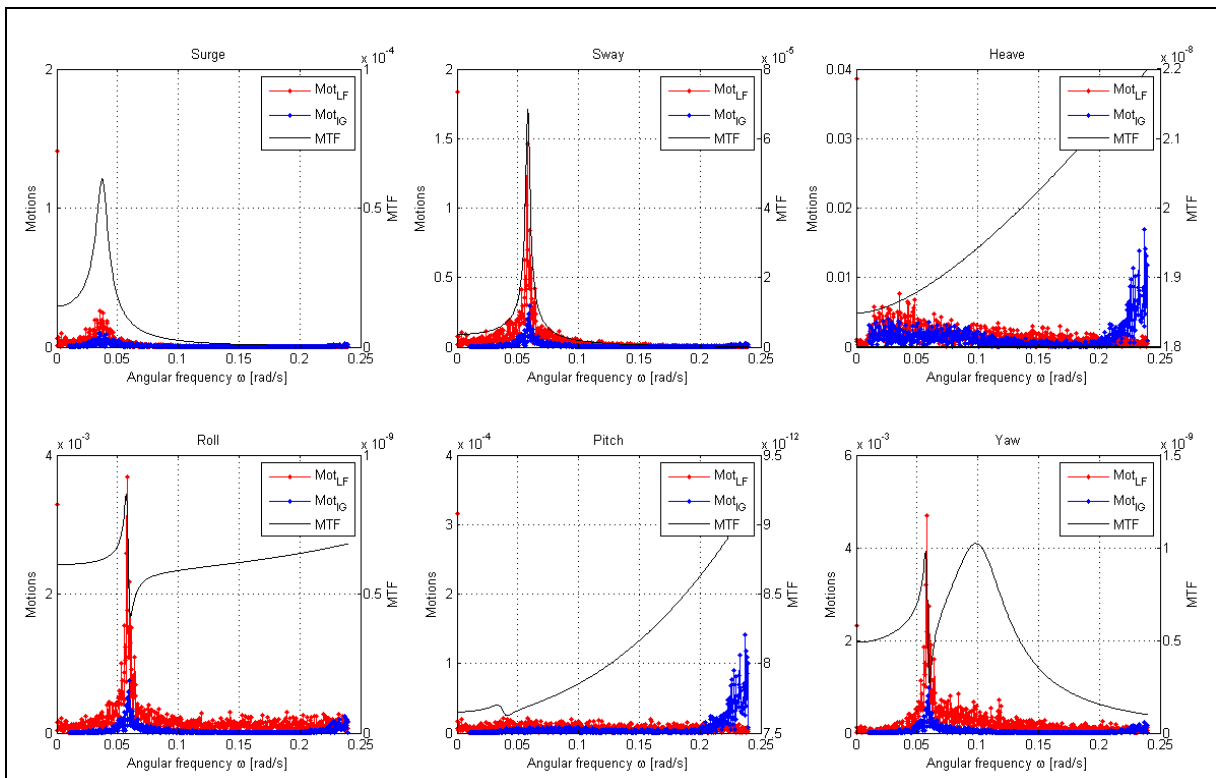


Figure 5.16: FPSO; Low frequency motions and MTF, 07/01/2014, 00h-03h.

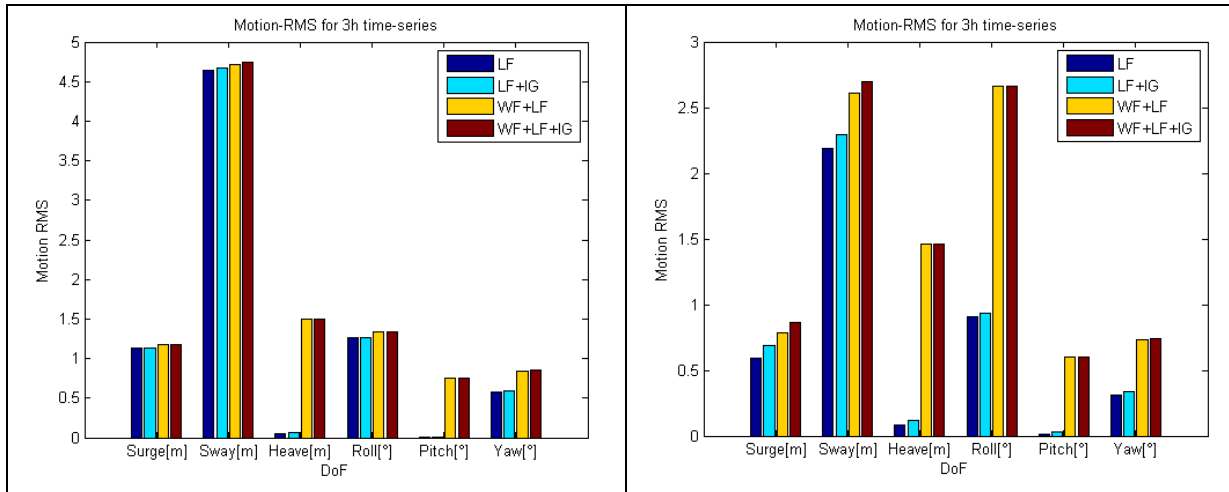


Figure 5.17: FSRU; Motion time series (3h), RMS, WF+LF vs. WF+LF+IG
 Left: 24/12/2013 06h-09h Right: 07/01/2014 00h-03h.

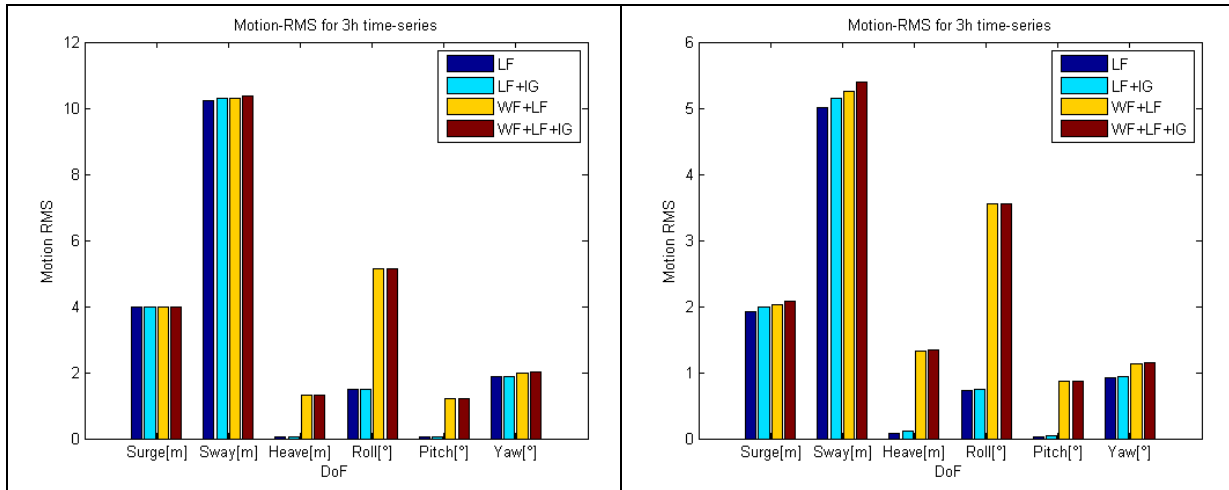


Figure 5.18: FPSO; Motion time series (3h), RMS, WF+LF vs. WF+LF+IG
 Left: 24/12/2013 06h-09h Right: 07/01/2014 00h-03h.

5.6 Directional sensitivity

The Force-RAOs and the QTF are strongly dependent on the wave incidence (see RAOs Figure 5.5 and Figure 5.6). For both IG events the dominant directions for swell and free IG waves are 290° and 130°, respectively. Different to the standard orientation (bow facing North), the directional sensitivity to swell and free IG waves was tested for 36 directions α , with $\alpha[^\circ]=0:10:350$. The resulting incidence angles for the swell and free IG waves differ accordingly. Figure 5.19 shows the orientation compared to the standard orientation. Also, the definition of *Surge* and *Sway* change accordingly.

Figure 5.20 and Figure 5.21 show the RMS values (similar to the results presented in the previous section, GWLF vs. GWLFIG) of the reconstructed motion time series for all 36 orientations for the FSRU and the FPSO floater, respectively.

As another comparison, the extreme values of the 3h duration time series are presented for all 36 orientation angles (GWLF vs. GWLFIG). While Figure 5.22 and Figure 5.23 show the results for FSRU and FPSO for the IG event on 24/12/2013 06h-09h, Figure 5.24 and Figure 5.25 show the results for both structures on 07/01/2014, 00h-03h.

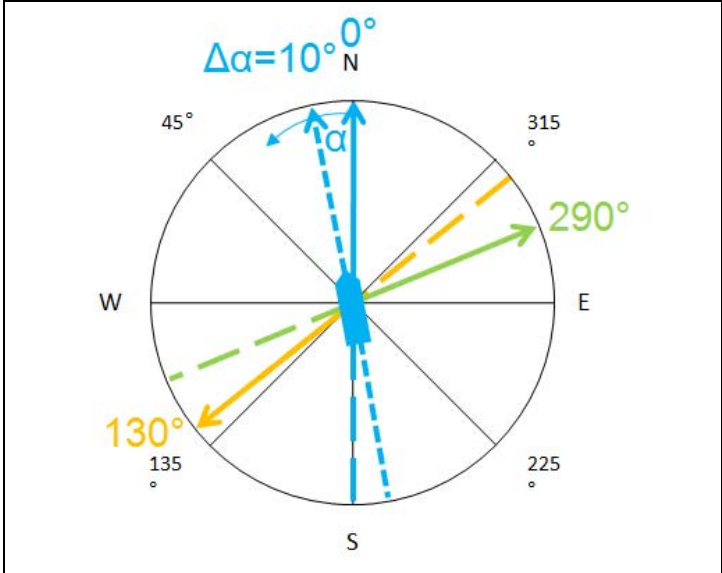


Figure 5.19: Orientation for directional sensitivity tests vs. standard orientation.

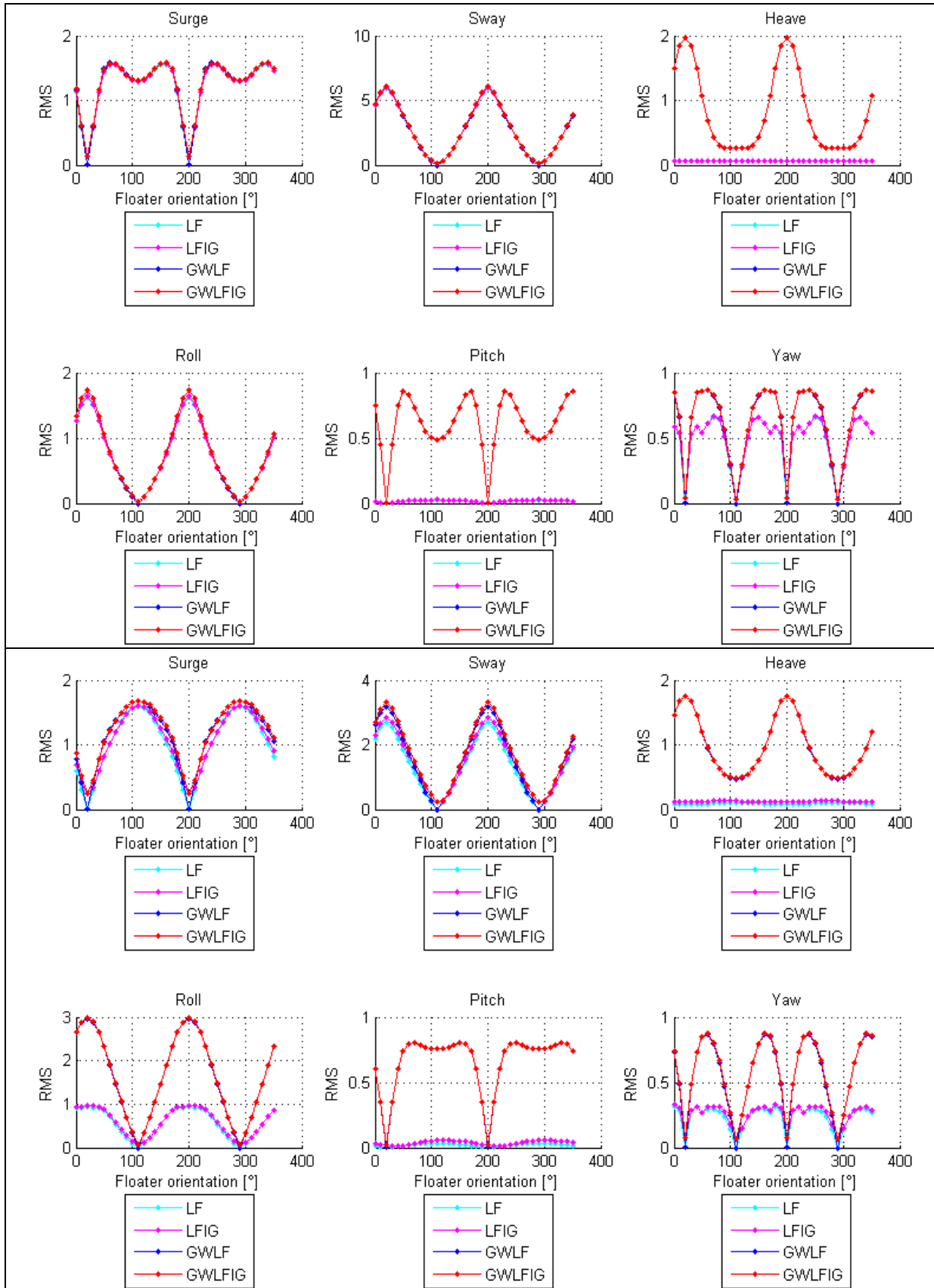


Figure 5.20: FSRU, Motion RMS values for different floater orientations

Top: 24/12/2013 06h-09h - Bottom: 07/01/2014 00h-03h.

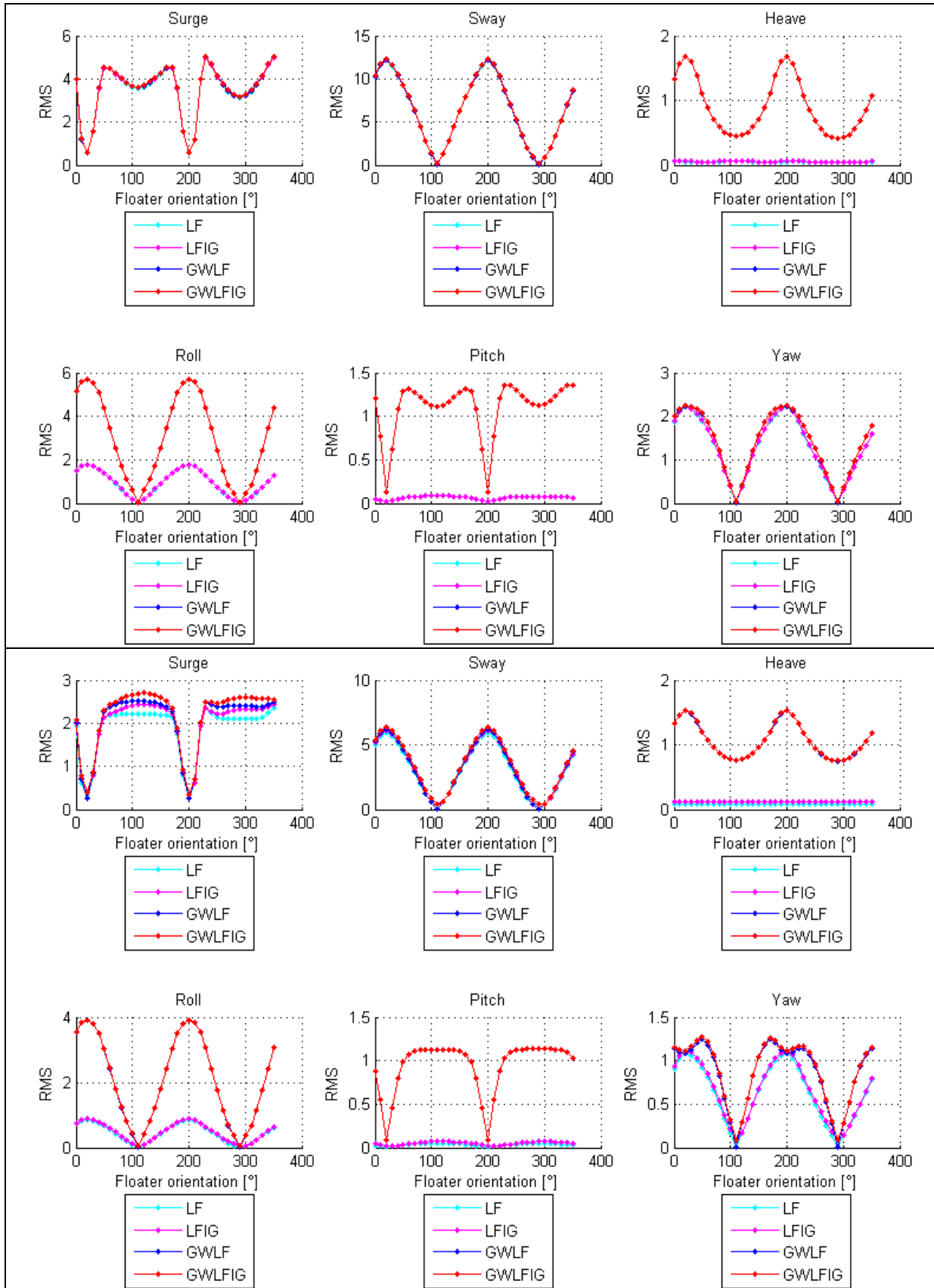


Figure 5.21: FPSO, Motion RMS values for different floater orientations

Top: 24/12/2013 06h-09h - Bottom: 07/01/2014 00h-03h.

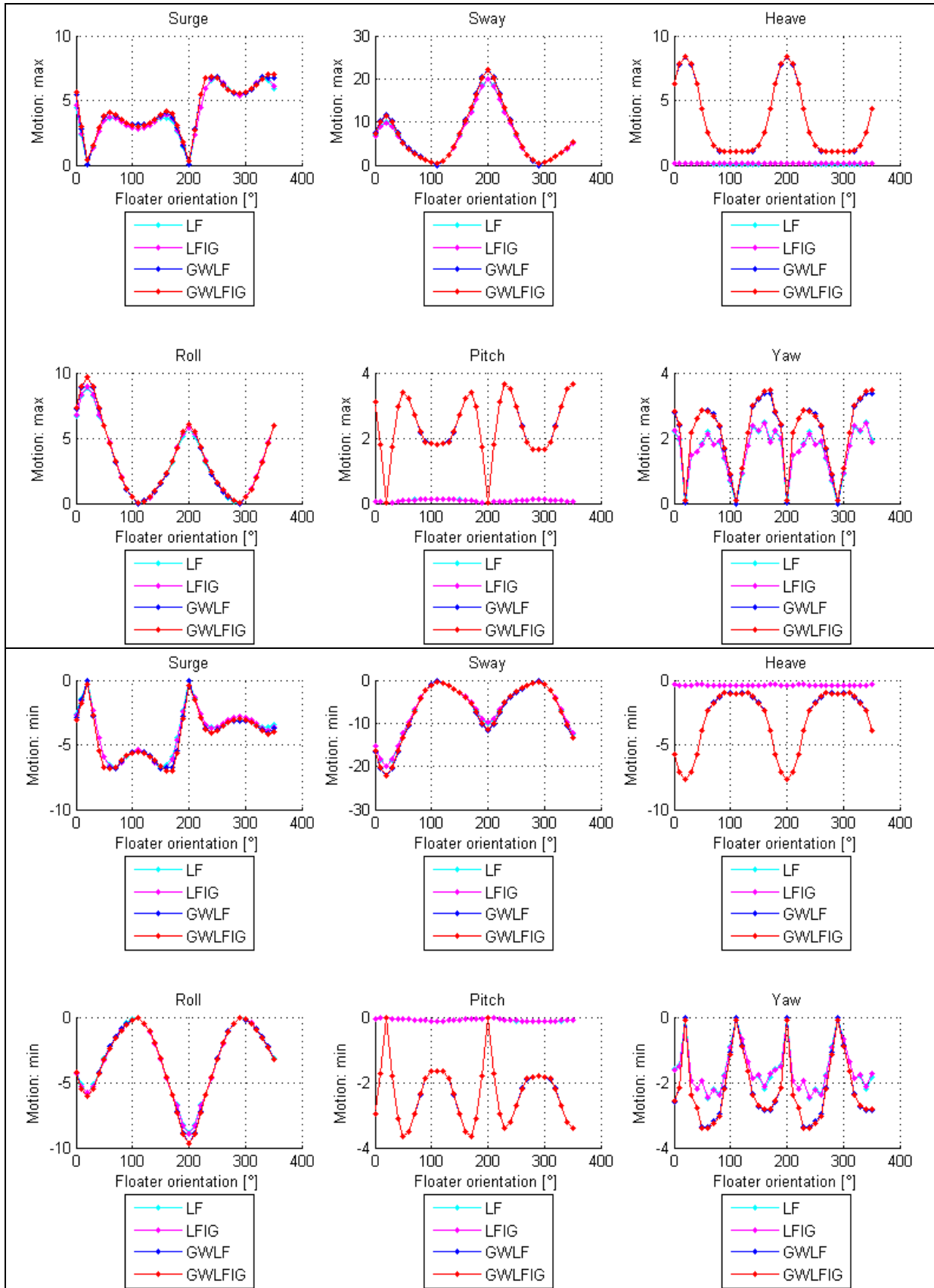


Figure 5.22: FSRU, Extreme values (motions), 24/12/2013 06h-09h.
Top: Max - Bottom: Min.

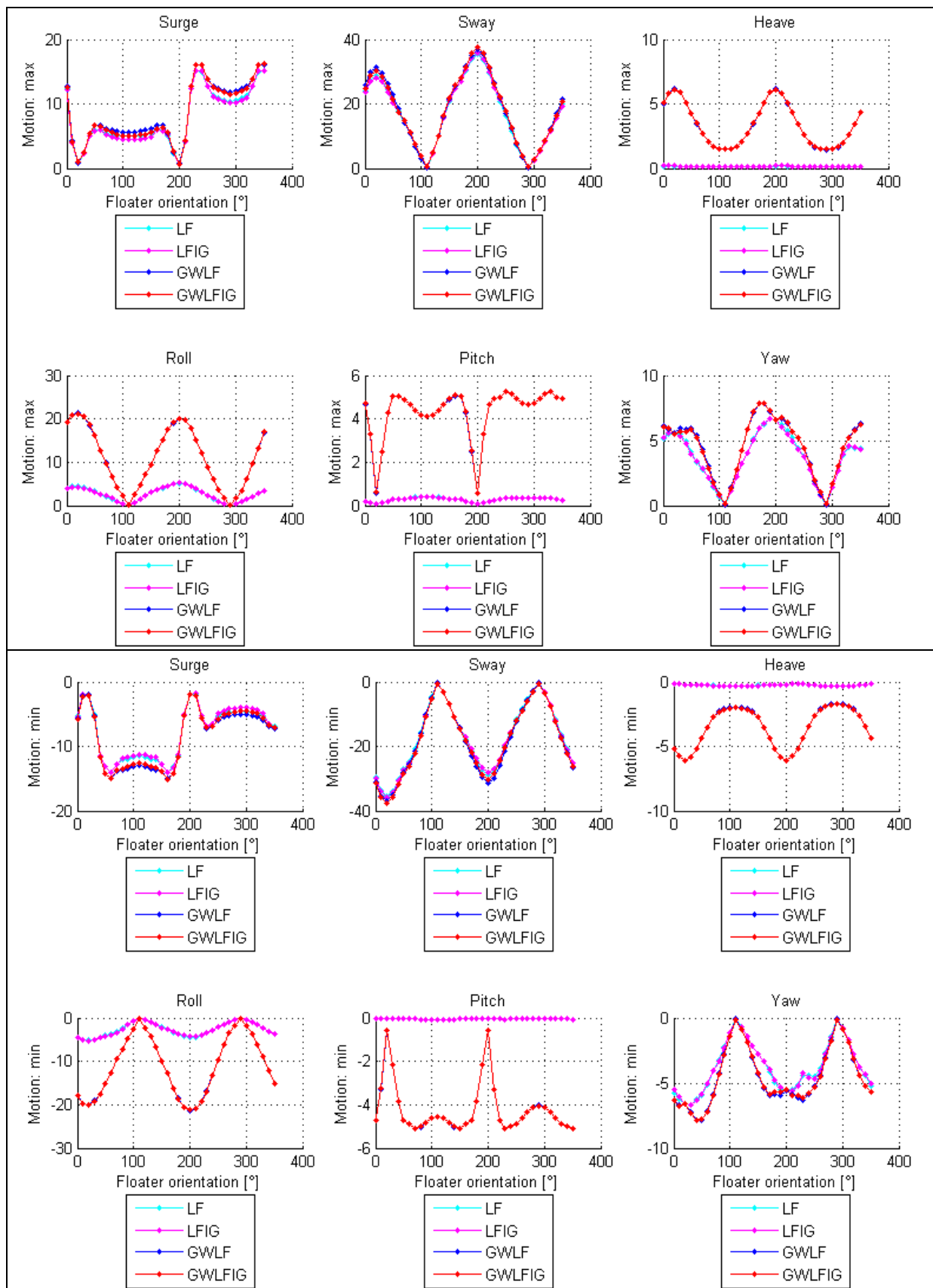


Figure 5.23: FPSO, Extreme values (motions), 24/12/2013 06h-09h.
 Top: Max - Bottom: Min.

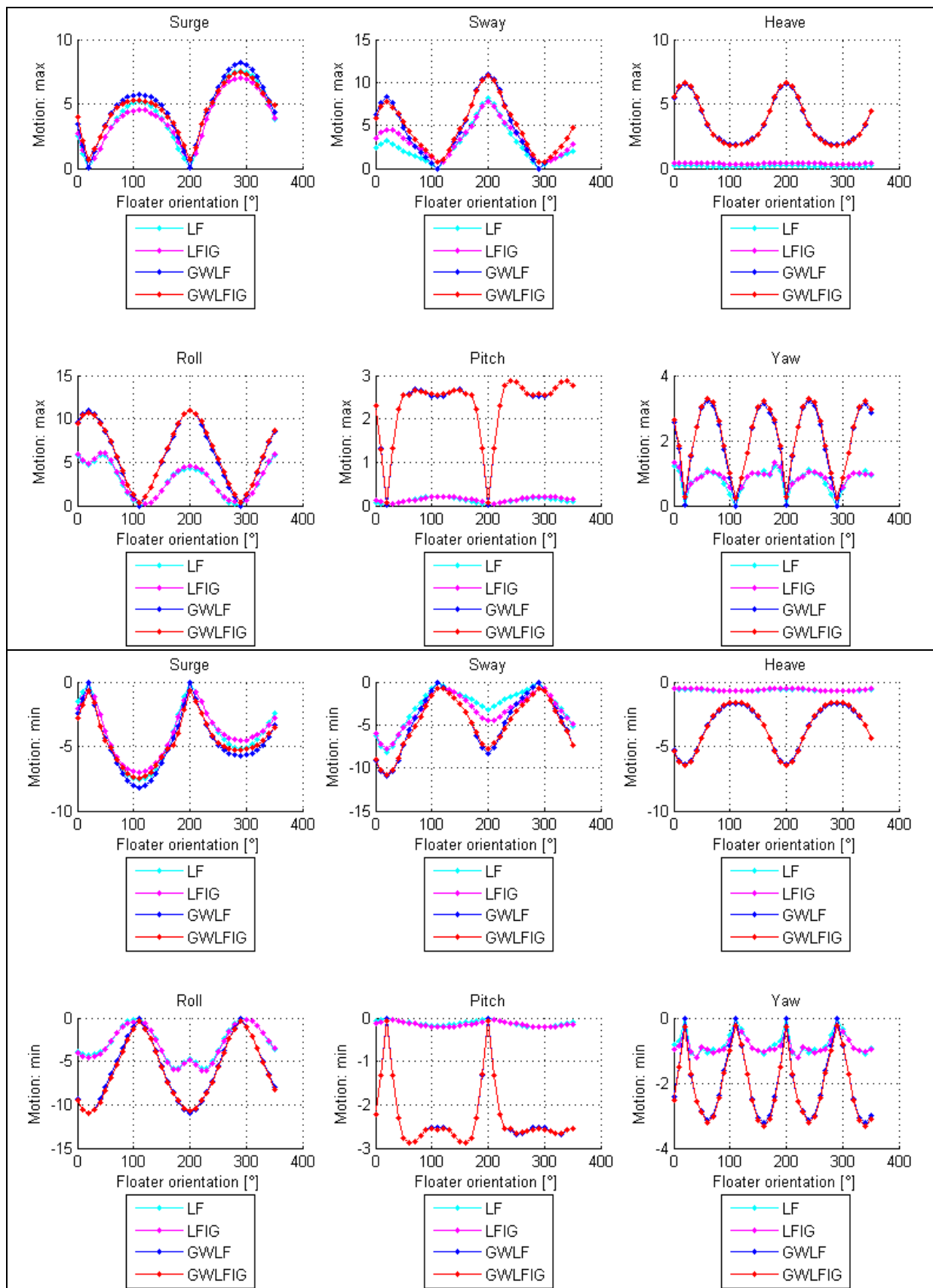


Figure 5.24: FSRU, Extreme values (motions), 07/01/2014 00h-03h.
 Top: Max - Bottom: Min.

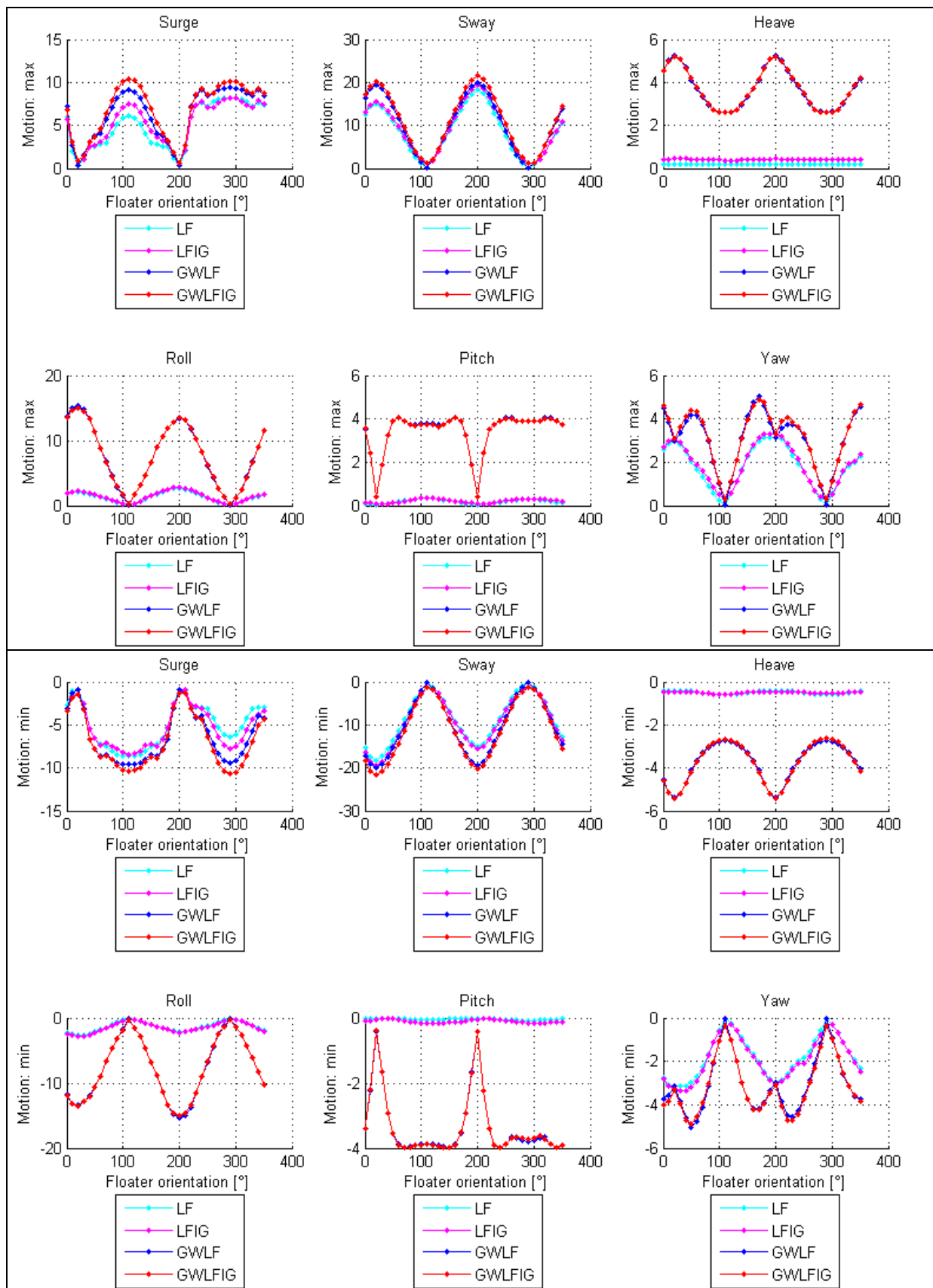


Figure 5.25: FPSO, Extreme values (motions), 07/01/2014 00h-03h.
 Top: Max - Bottom: Min.

6 Summary and conclusions

In order to evaluate the importance of free IG waves to moored floating structures at a specific test site (SEM-REV), two important IG events (24/12/2013 06h-09h and 07/01/2014 00h-03h) have been selected, and were tested with two different floaters and mooring systems (FSRU and FPSO).

While the motion response to first order wave forces, at the wave frequencies, and to second order low-frequency forces, coming from the non-linear interaction of different wave frequencies (at difference frequencies) were obtained according to standard design-guidelines, the implementation of free IG waves was a novel in this study.

Even though free IG waves are a result of non-linear interaction of wave groups travelling over long distances they are treated here as "linear waves" and the standard linear transfer function (LTF) for the wave forces was used.

Finally, the motion response to these additional low-frequency wave forces was obtained using the same mechanical transfer function (MTF) of the floater-mooring-systems (FSRU and FPSO), as for the standard procedure described above.

The input for all the calculations were directional wave spectra, including the low-frequency IG frequency range (see Section 4.1). After identification of the dominant incidence directions for the standard wave frequency range and the IG frequency range, respectively, the directional wave spectra were integrated over the directions to obtain a one-directional wave spectra. While the first order wave forces (WF) and the second order low-frequency forces (LF) were used together with the dominant swell direction (290° in both IG events), the wave forces due to free IG waves (IG) were used together with the dominant free IG wave incidence direction (130°). This "pseudo-directional" approach is a simplification of an otherwise multidirectional solution. The use of only one direction for the swell together with standard 2D-QTF, allowed for the implementation of the efficient sum-over-diagonals method, substituting the double sum for the second-order low-frequency forces.

The complete methodology applied in this study included the following:

- Calculation of directional wave spectra including the low IG frequencies using the WAVEWATCHIII model's IG1 switch for two selected IG events for the SEM-REV test site location.
- Identification of dominant wave incidences for swell and free IG waves.
- Calculation of complete hydrodynamic coefficients for two floaters and their specific mooring system using Bureau Veritas' HYDROSTAR software . Verification against available test data in the FSRU case and verification against available test results from earlier projects in the FPSO test case.
- Calculation of first-order (WF) and second-order wave forces (LF, IG) in frequency space and reconstruction of 3h duration time series.
- Calculation of motion response using one mechanical transfer function in frequency space and reconstruction of 3h duration time series.
- Comparison of wave forces and resulting motions, separately and combined.

The following conclusions regarding the importance of taking into account free Infragravity waves to moored floating structures were obtained during this study:

1. The importance of free IG waves is clearest comparing the low-frequency wave forces (LF vs. IG), see Figure 5.9, Figure 5.10, Figure 5.11 and Figure 5.12. Because the same mechanical transfer function for LF and IG forces is used, difference in motion response is directly predictable. For both selected moored floating structures and both IG events the LF forces are dominant.
2. The effect of free IG waves could be shown, but their importance strongly depends on the shape and magnitude of the QTF, related to the selected floater-mooring-system.
Comparing the example Surge-QTF for 290° wave incidence (see Figure 5.7 and Figure 5.8), both show strong values on the main diagonal and for the diagonals representing a difference frequency in the vicinity of the resonant frequencies for surge for both, FSRU and FPSO. The strong valued main diagonals lead to high values for the steady drift forces (zero-bins in Figure 5.9, Figure 5.10, Figure 5.11 and Figure 5.12) and ultimately to strong offsets in the motion time series reconstructions.

Other floater geometries (shallow draft, small members, multi-floaters, etc.) might show a different relation between LF forces and wave forces due to free IG, because of their very different QTFs. First-order wave forces, Motion RAO and QTF depend strongly on

the hull shape. With the existing spectrum of different floaters in marine-renewable energies and the oil-and-gas industry, very different results could be obtained. Also the mooring stiffness strongly affects the motion response.

3. Because both selected structures are ship-shaped, they are strongly sensitive to the incidence of incoming waves (see Figure 5.22, Figure 5.23, Figure 5.24 and Figure 5.25). Axis symmetric hull shapes together with symmetric mooring systems should exhibit a constant response for different wave incidences.
4. The two selected IG events, show similar significant wave heights, but the free IG wave height is almost two times bigger on the 01/01/2014, 00h-03h (see Figure 4.2 and Figure 4.3). This relation could not be shown in the motion response time series. Nonetheless, the inclusion of free IG waves to the motion response becomes clearly visible for the second IG event (see Figure 5.23 vs. Figure 5.25). It has to be stated, that the sharp definition applied for the f_{IG} limit of 0.04 and the low peak frequency of the swell for the IG event on 07/01/2014, means that some wave energy of the swell is treated as free IG energy. This can be seen clearly in Figure 5.10, Figure 5.12, Figure 5.14 and Figure 5.16. The frequencies where this happens are well outside the resonant peak of the mechanical transfer function. Therefore, no further adjustments were done to the calculations.
5. The pseudo-directional approach used in this study is considered fairly conservative, as for a floater orientation $\alpha=20^\circ$ it means all the swell is hitting the ship-shaped hull as beam-seas, together with the IG wave hitting it at about 110° . Considering the hull shape of both structures and their Force-RAOs (see Figure 5.5 and Figure 5.6), as most violent condition. On the other hand, the use of 2D-QTF might slightly under-predict the second-order LF forces in reconstructed time series (Rezende *et al*, 2010), which would speak in favor for using full directionality and 4D-QTF. In this study though, use was made of the effective sum-over-diagonals method (see Section 3.3), using 2D-QTF, which allowed to by-pass memory and computational problems during the calculation of second-order LF forces.
6. The WAVEWATCHIII model is capable of providing valuable results for free IG waves for any location of interest. Nonetheless, the results represent a novel empirical approximation and fairly little field data is available to cross-check them. The factors for calibration of the IG module, the resolution of the reflective boundary (coast) and the resolution of the bathymetrical map used to obtain the presented results might be a source of error. While the magnitude of free IG waves for the SEM-REV test site used for this

study was found to match field data for the period of January 2014 (comparison is not part of this report), the directional information might be of question. Considering the sensitivity to wave incidence for the selected floater-mooring-systems this might be of importance in the final conclusion regarding the importance of free IG waves to moored floating structures.

7. The direction wave spectra including the free IG frequencies, were calculated for constant water depths (see Section 4). The calculations were conducted for a global grid. Including tide variations possibly would increase the accuracy of the predicted wave spectra, but at a very high computational cost. Considering the depth sensitivity of QTF and the tidal range at SEM-REV, this should be the subject of future work.
8. The presented results for the 3h duration time-series do not include a correction for large displacements (*surge, sway*) or rotations (*heave*). Although this correction would increase the precision of the reconstructed time-series, we think the general conclusions would not be affected.
9. One limiting factor for the selection of suitable floater-mooring-systems for testing was the availability of additional damping coefficients, usually obtained in physical model tests. Radiation-diffraction codes like Bureau Veritas' HYDROSTAR need additional information for the damping. Otherwise the obtained motion RAOs at the resonant frequencies will be unrealistically high, as the standard radiation damping is very low at these frequencies. Additional information for the low-frequency damping, e.g. wave-drift-damping and viscous-damping, is required for realistic results.

New capabilities in wind/wave modeling like the IG module in WAVEWATCHIII, allow for an inclusion of free IG waves into design considerations for new floater-mooring-system designs. Nonetheless, it should be noted that the empirical factorization of the free IG wave energy is still an approximation and fairly novel. Ultimately this study cannot give an overall answer to the importance of free IG waves to moored floating structures, but a methodology is presented for future implementation in standard design procedures. Only two important IG events have been investigated. The similarity of the two wave spectra though suggests that there are more free IG events with maybe more energetic free IG waves. Also, the selection of the two floater-mooring-systems does not allow for a final conclusion over all kinds of different floaters in a general way.

7 Future work

The initial purpose of this study was to evaluate the importance of free IG waves at the SEM-REV test site for a specific moored floating structure; a state-of-the-art floating offshore wind turbine (FOWT), with concrete floater including a moon pool. Figure 7.1 shows an artistic description of the future FOWT. Until the end of this study not enough information was available for applying the presented methodology to this special floater-mooring-system. While the floater is almost axis symmetric, the mooring system, consisting of rope-chain lines, is not.

In order to apply the presented methodology to this floater-mooring-system the following information is requires:

- Full mass-inertia matrix
 - Full additional stiffness matrix (mooring system representation)
 - Additional damping coefficients (wave drift and viscous damping)
- The floater features a heave plate/lip. This and the sharp 90° edges of the floater require special attention.

The effect of the moon pool also requires special attention.



Figure 7.1: Ideol floating offshore wind turbine (credit: Ideol).

Apart from the application of the presented methodology to the Ideol FOWT, several open points to be studied in continuation to this project have been identified.

1. A more generic study could investigate the relation LF forces vs. forces due to free IG for structures with comparable characteristics, such as: mass-inertia, mooring-stiffness, additional damping... This might give direct insight on the influence of hull shapes for example. This study would require physical model tests, or CFD studies to obtain the additional low-frequency damping. This kind of study could answer the question on the importance of free IG waves to moored floating structures in a general way better, than the present study.
2. As mentioned in the previous section, the resolution of the grid and the bathymetry used for the WAVEWATCHIII calculations might be a source of error and could be analyzed.
3. The present study treats the free IG waves as Airy waves in terms of possible linear superposition out of practical reasons. In reality, the free IG waves on the Armorican shelf are shallow water waves. The differences in assumptions could be part of a future study.
4. The directional wave spectra obtained for this study differ slightly from the directional wave spectra found in the HOMERE database. Both calculations are obtained with different parameters (wind fields, tides, bathymetry/sediments, etc).

Initially, wave spectra for 2008 were tested in this study (since HOMERE data was available). Figure 7.2 shows a simple comparison of the directional spectral variance density $S(f,\theta)$ for the W0027N472 export node for the 10/03/2008, between 00h and 12h. On top the two 3h wave spectra from the global grid IG calculations (see Rawat, 2015) are shown, while on bottom the 1h time wave spectra from the HOMERE calculations for the center hour interval are shown. The red segmented line marks the difference in low-frequency for the two different calculations.

The many differences in the two calculations should be analyzed further, since the conclusion on the importance of free IG waves to moored floating structures depends on the correct application of wave energy in the "classical" wave frequencies above the free IG frequency limit of 0.04 Hz.

5. With the availability of the HOMERE database an identification of important IG events for the SEM-REV test site could be conducted on the base of similarities to the two IG events presented in this study. This could be of interest for the future prediction of free IG waves, as at the moment the presented study relies on reanalysis results.

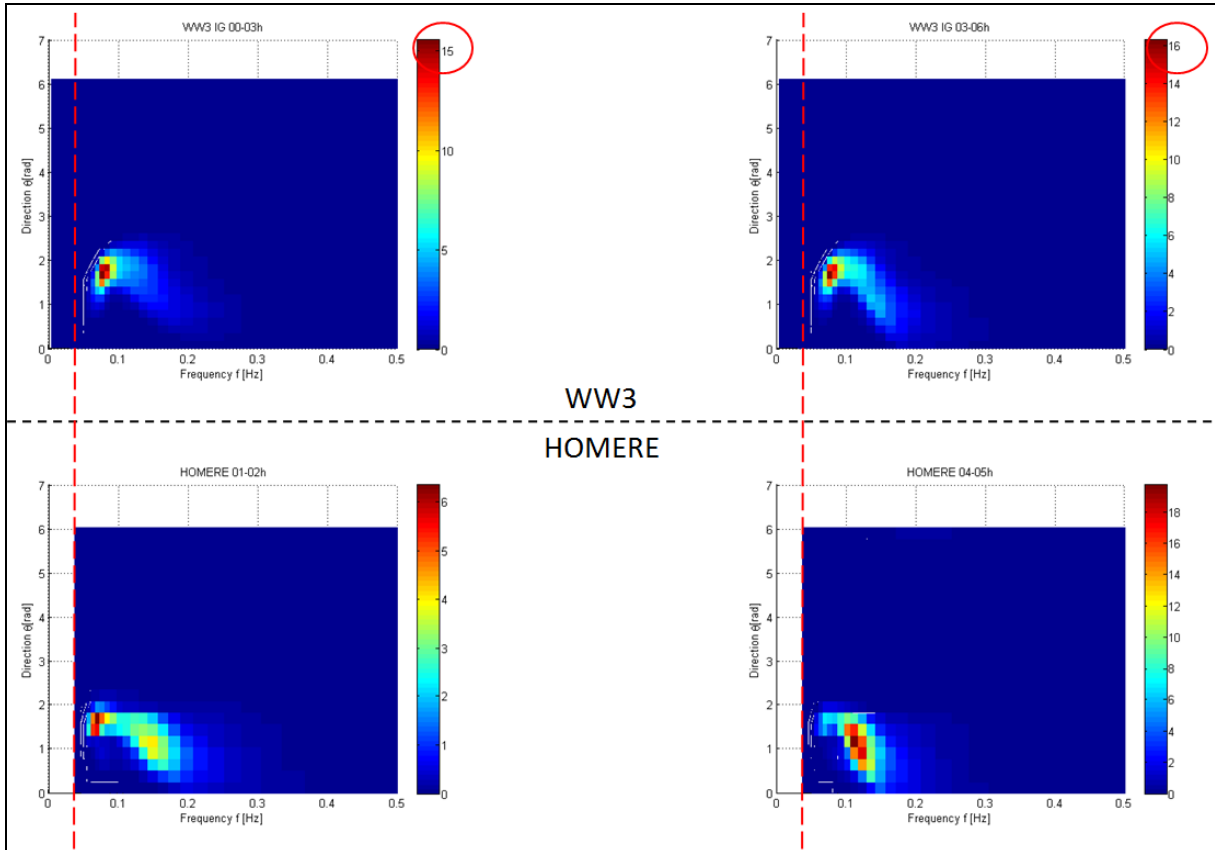


Figure 7.2: W0027N472; Directional spectra; WW3 vs. HOMERE; Date: 10/03/2008; 00h – 06h.

8 References

- Ardhuin, F., Rawat, A., Aucan, J., 2014, '*A numerical model for free infragravity waves : definition and validation at regional and global scales*', *Ocean Modelling*, 2014, 77, p.20-32.
- Munk, W. H., 1950, '*Origin and generation of waves*', Proceedings 1st International Conference on Coastal Engineering, Long Beach, California: ASCE, pp.1-4.
- Prevosto, M., 2010, '*A priori simulation of forces and distribution of extrema*', CHEEPP2 WP2: Local effects, Ifremer project report R01HO10.
- Rawat, A., 2015, '*Numerical Modelling of Infragravity waves: From regional to global scales*', PhD Thesis.
- Rezende F.C., Chen X., 2010, '*Approximation of second-order low-frequency wave loading in multi-directional waves*', Proceedings of the ASME 2010 29th International Conference on Ocean, Offshore and Arctic Engineering, OMAE2010, June 6-11, 2010, Shanghai, China.
- Tolman, H. L. and TheWAVEWATCH III R^o Development Group, 2014, '*User manual and system documentation of WAVEWATCH III[®] version 4.18. Tech. Note 316*', NOAA/NWS/NCEP/MMAB, 282 pp. + Appendices.

Appendix A - FPSO: Reproduction of available data.

This study was initially about the Ideol FOWT, but the first structure tested was FSRU floater-mooring-system. Due to the unavailability of the Ideol data, another floater-mooring-system was selected. The data for the FPSO from the CITEPH-CHEEPP2 project was available, including the low-frequency damping. The available data was obtained with the radiation-diffraction code DIODORE. Apart from the available data, the methodology presented in this study required the force- and motion-RAOs for the free IG frequencies. For the present study the complete force- and motion RAOs, QTF and the coefficients for added masse and radiation damping were recalculated using Bureau Veritas' HYDROSTAR.

While the general characteristics for this floater are presented in Section 4.2.2, the original DIODORE results were calculated for a vertical position of the centre of gravity $CoG_Z[m] = -20.02m$. The first intents to reproduce the original results were unsuccessful. With the given mesh-file the hydrostatics were checked. Table A. 1 shows the comparison between HYDROSTAR and original DIODORE results using the original CoG_Z , while Figure A. 1 shows the water plane area A_w . With this information the hydrodynamic stiffness matrix was cross-checked. Table A. 2 shows the results for the 6x6 matrices. The DIODORE results show some inconsistencies with the available mesh-file.

The correct reference point and coordinate system was verified in the correct reproduction of the 36 frequency dependent results for the added mass and the radiation damping (see Figure A. 2 and Figure A. 3). With these results it was possible to recalculate the original force- and motion-RAOs (see Figure A. 4, Figure A. 5 and Figure A. 6).

Waterplane area A_w [m²]:	5378.9			(HYDROSTAR)
Cetroid (X_c, Y_c) [m]:	3.776 0.000			(HYDROSTAR)
I_{xx} :	0.40755E+06	BM_{xx} :	9.28464	(HYDROSTAR)
I_{xy} :	0.00000E+00	B_{mxy}:	0.00000	(HYDROSTAR)
I_{yy} :	0.13250E+08	B_{myy}:	301.86232	(HYDROSTAR)
Hull volume [m³]:	43895			(HYDROSTAR)
	43895.711			(DIODORE)
Center of Buoyancy (wrt CS):	5.788 0.000 -4.187			(HYDROSTAR)
	5.7842 0.000 -4.1797			(DIODORE)
Centre of gravity (wrt CS):	5.6700 0.000 -20.020			(HYDROSTAR)
	5.6700 0.000 -20.020			(DIODORE)
Reference point (wrt CS):	5.6700 0.000 -20.020			(HYDROSTAR)
GM_{xx} , GM_{yy} :	25.09441, 317.628009			(HYDROSTAR)
Rho (water) [kg/m³]:	1018			

Table A. 1: FPSO; Hydrostatics, original CoG_Z .

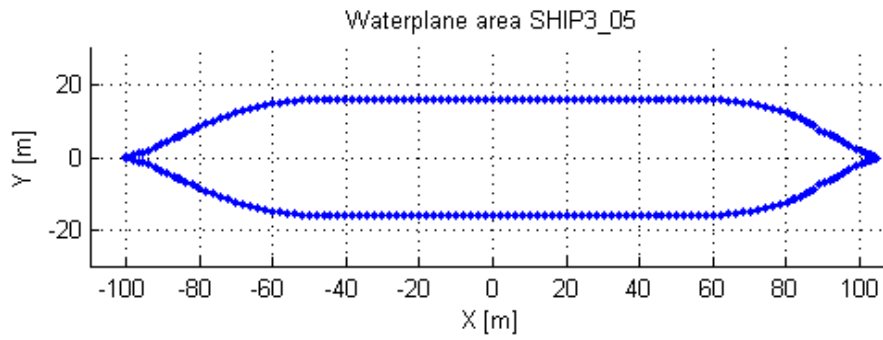


Figure A. 1: FPSO, water plane area A_w .

Hydrodynamic stiffness - DIODORE:

0	0	0	0	0	0
0	0	0	0	0	0
0	0	5.37E+07	0	0	0
0	0	0	6.94E+09	0	0
0	0	0	0	6.94E+09	0
0	0	0	0	0	0

Hydrodynamic stiffness - Hydrostar:

0	0	0	0	0	0
0	0	0	0	0	0
0	0	5.37E+07	0	103770000	0
0	0	0	1.1E+10	0	0
0	0	1.04E+08	0	1.392E+11	0
0	0	0	0	0	0

Hydrodynamic stiffness - Manual:

0	0	0	0	0	0
0	0	0	0	0	0
0	0	5.37E+07	0	1,02E+08	0
0	0	0	1.10E+10	0	0
0	0	1.02E+08	0	1.41E+11	0
0	0	0	0	0	0

Table A. 2: FPSO; Hydrostatic stiffness matrix.

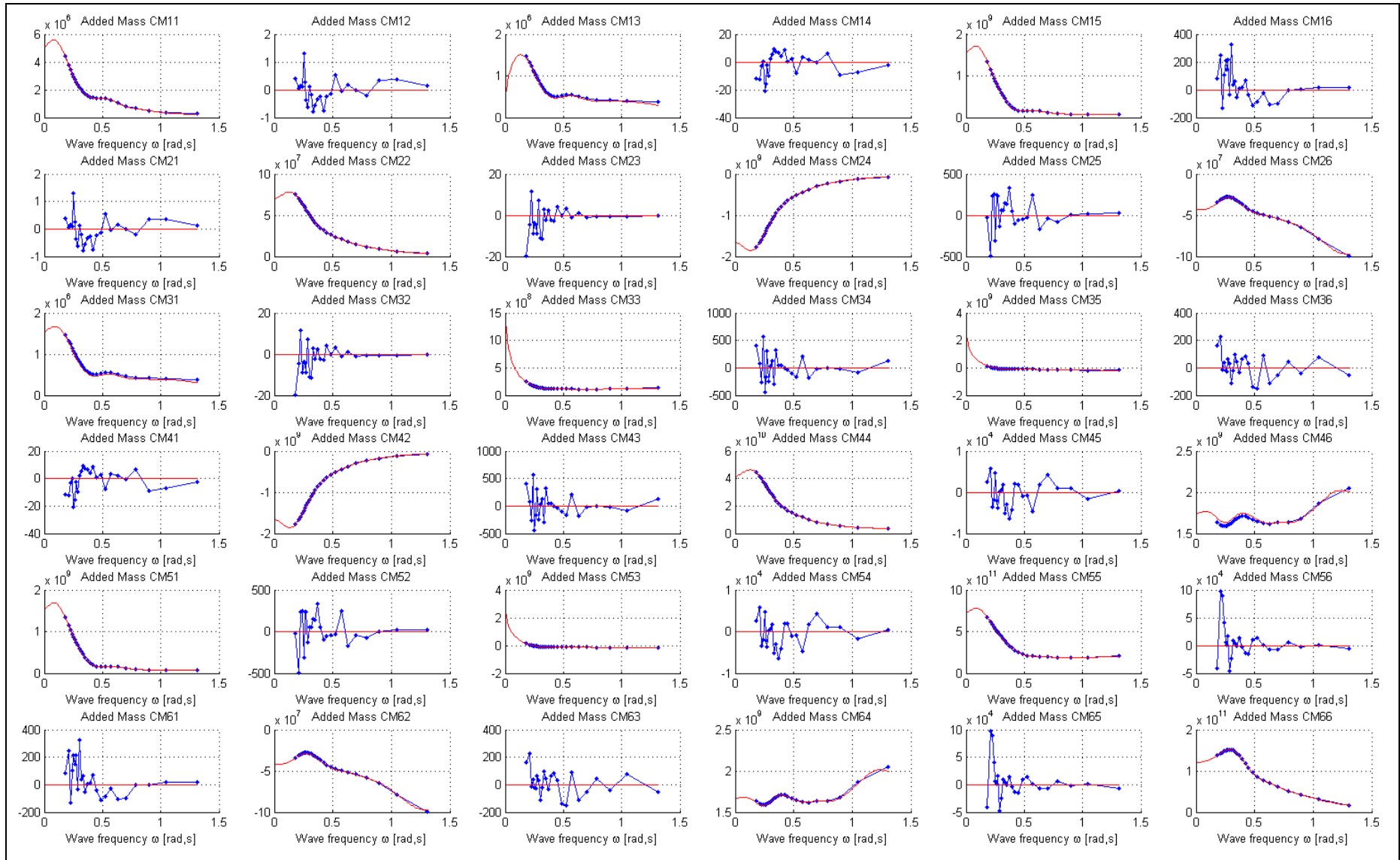


Figure A. 2: FPSO; Added masses, HYDROSTAR (red) vs. DIODORE (blue), CoG_Z=-20.02m.

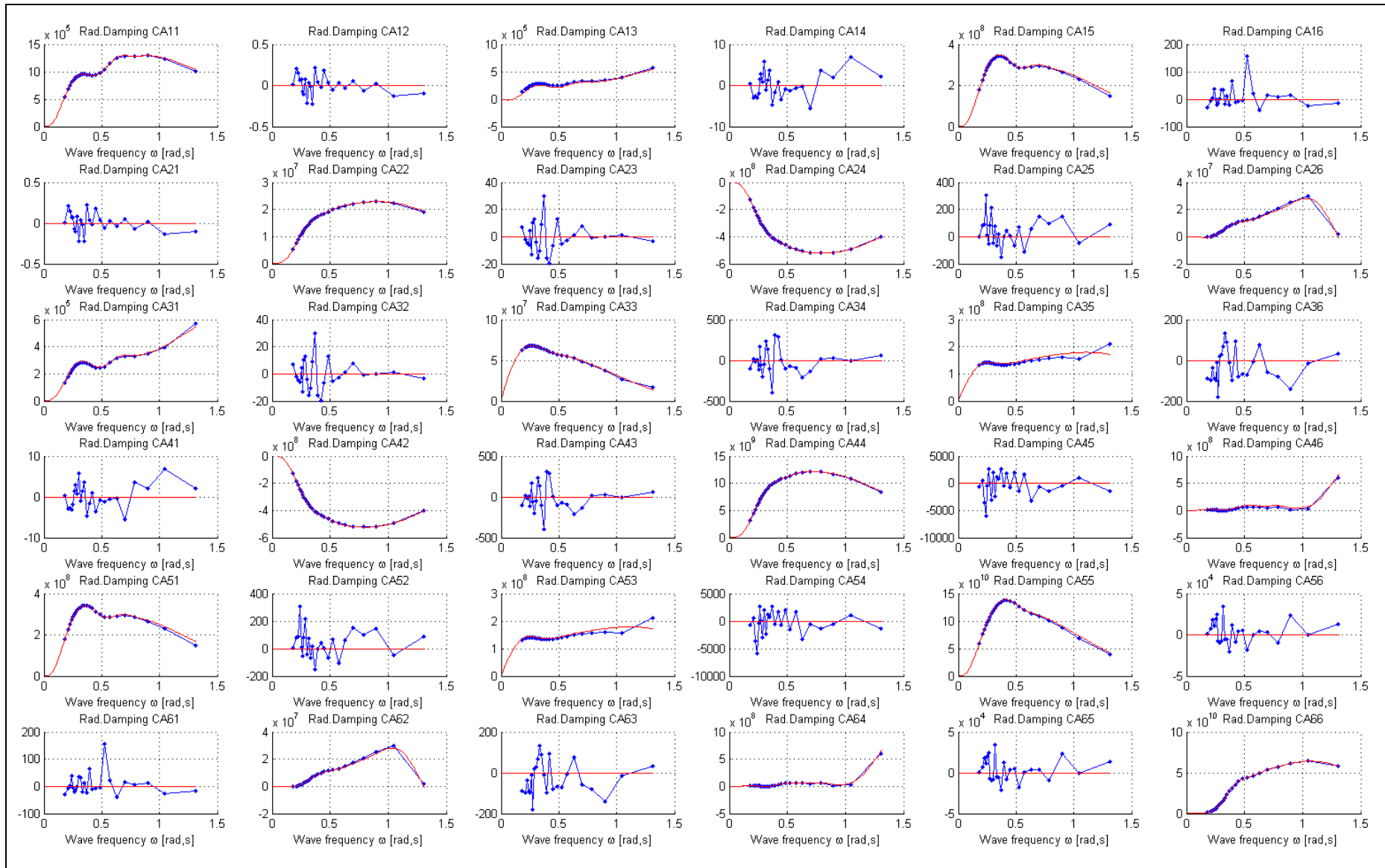


Figure A. 3: FPSO; Radiation damping, HYDROSTAR (red) vs. DIODORE (blue), CoG_Z=-20.02m.

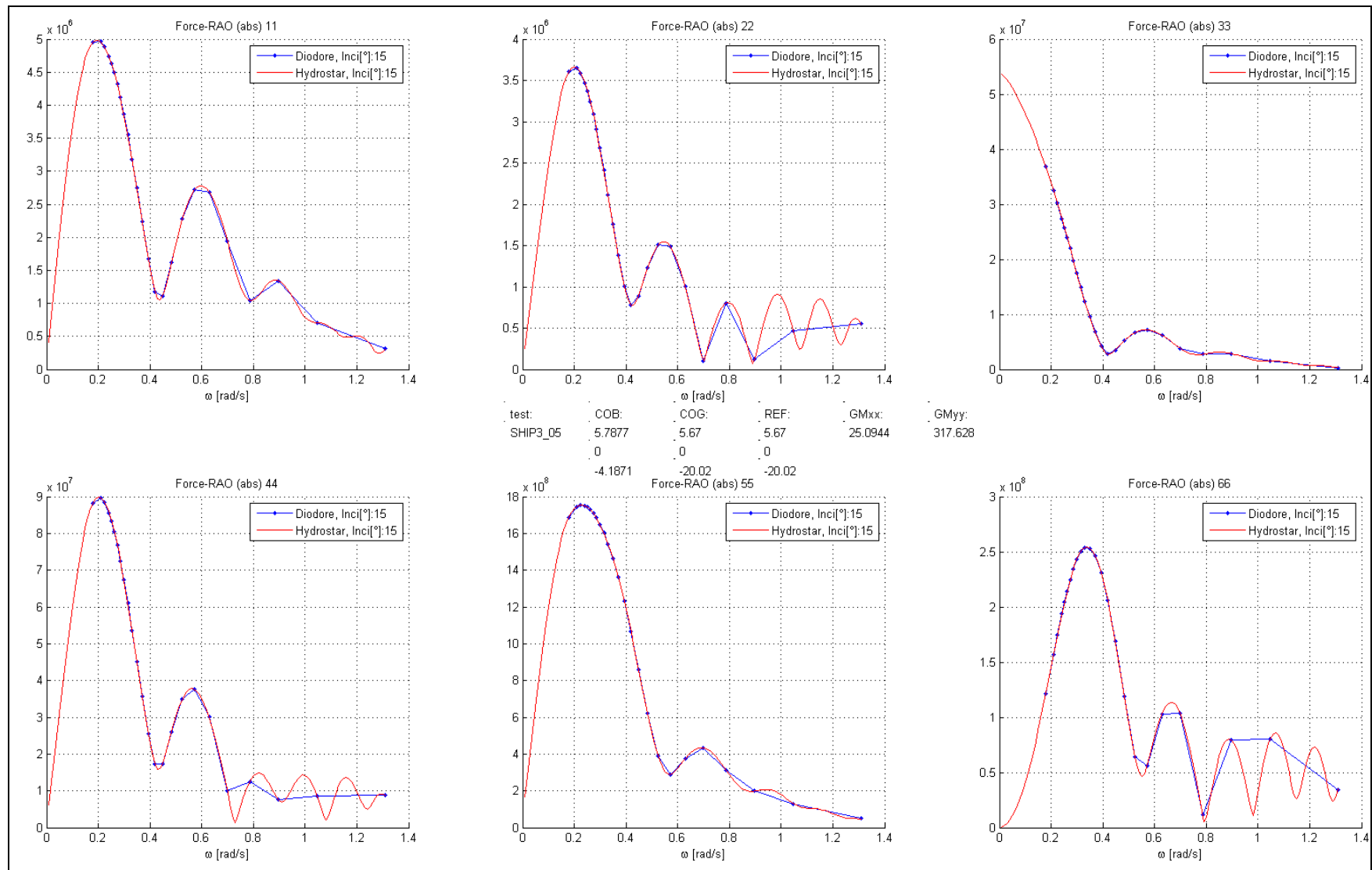


Figure A. 4: FPSO; Force-RAOs, HYDROSTAR (red) vs. DIODORE (blue).

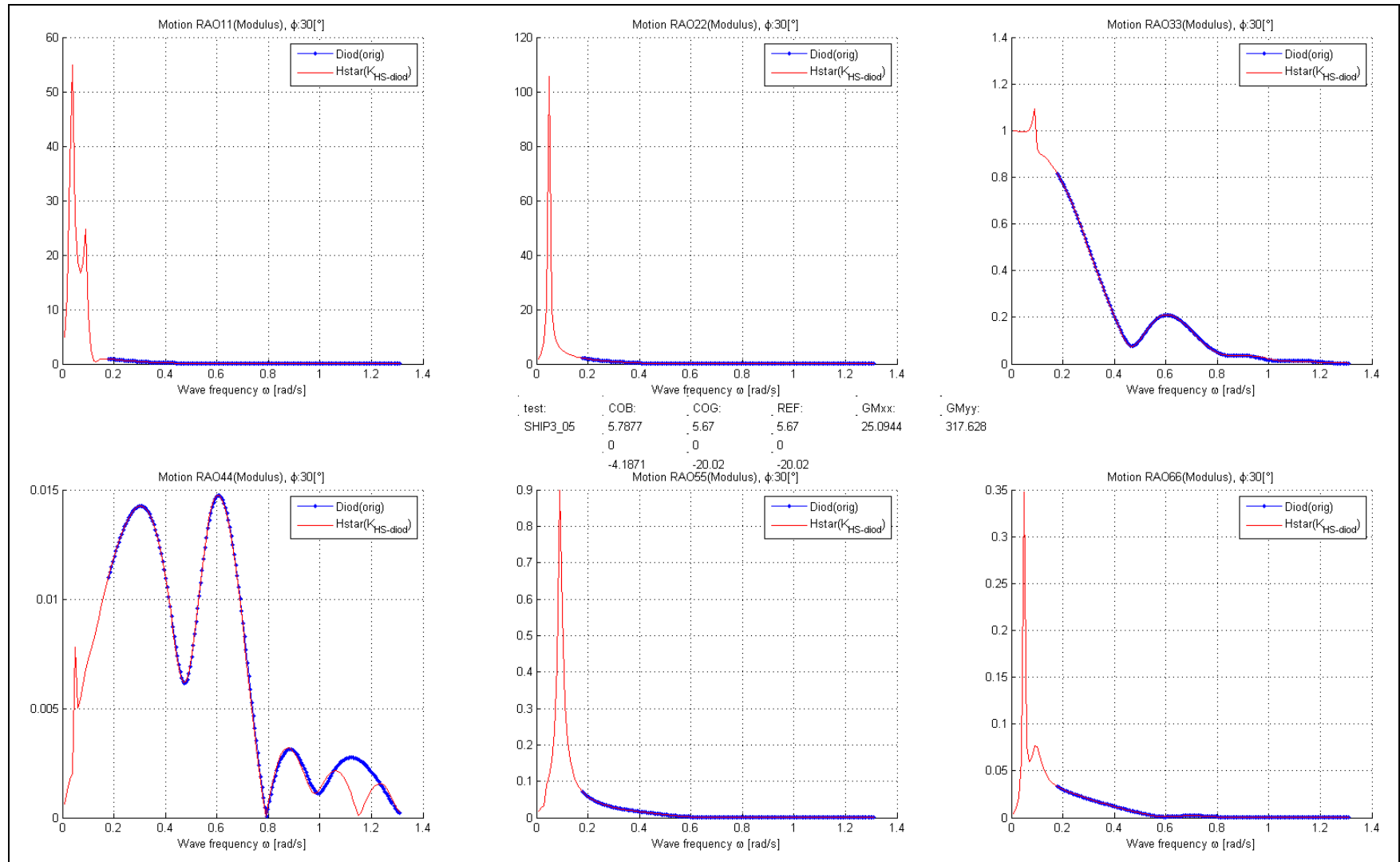


Figure A. 5: FPSO; Motion-RAOs, HYDROSTAR- $K_{H-DIODORE}$ (red) vs. DIODORE (blue), using DIODORE's hydrostatic stiffness.

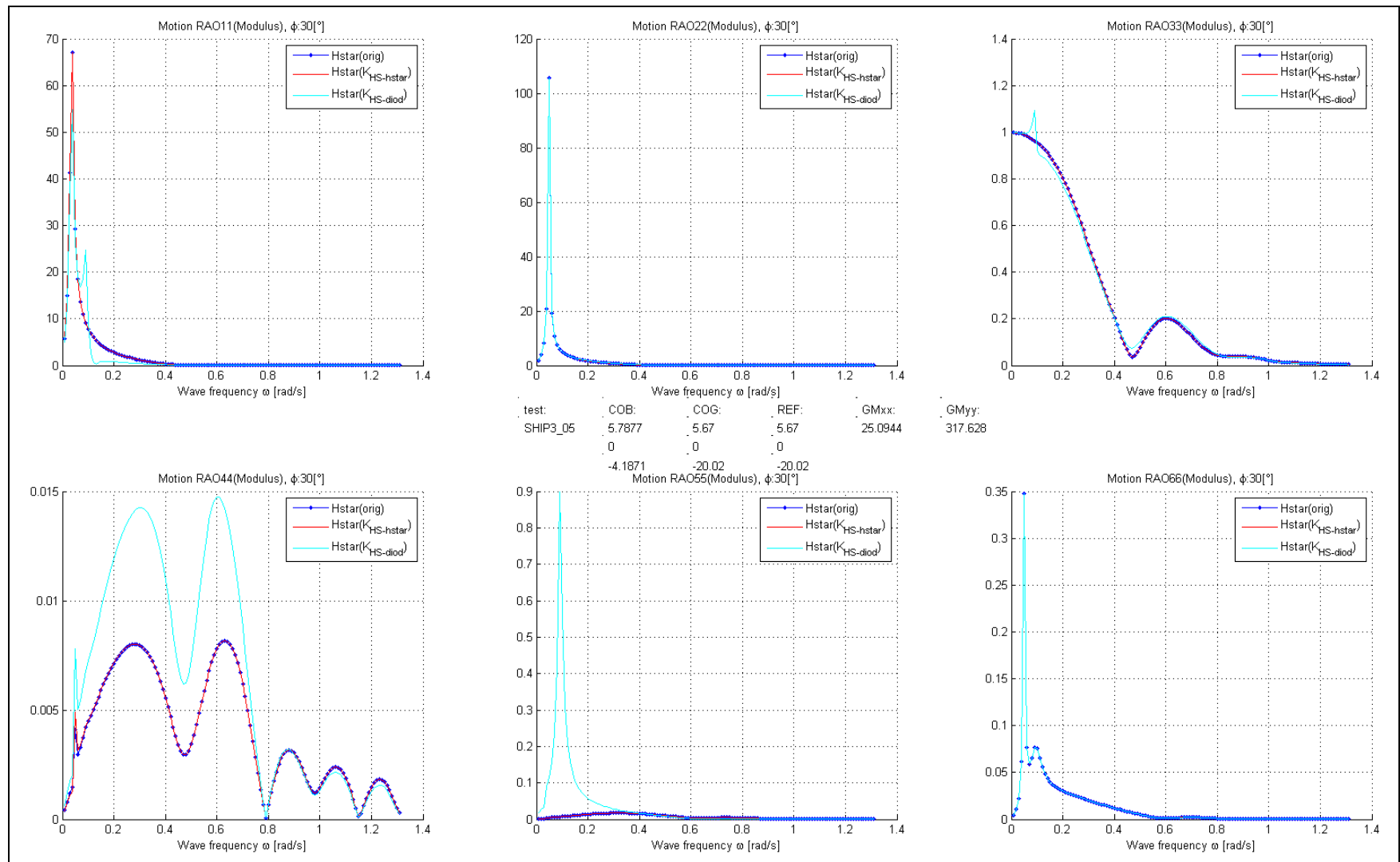


Figure A. 6: FPSO; Motion RAOs HYDROSTAR- K_H -DIODORE (red) vs. DIODORE (blue) vs. HYDROSTAR (cyan).

These results justified a complete new calculation of the force- and motion-RAOS, as well as the QTF, using the correct hydrostatic stiffness, as provided by HYDROSTAR.

Another issue with the original DIODORE data, was the vertical position of the CoG of -20.02m, resulting in a very high and unrealistic metacentric height GMxx of 25.1m. The FPSO BUMI - Armada Perkasa, being a modified tanker should have a metacentric height of about 1 to 6 m⁴. Running the hydrostatics module of HYDROSTAR with a different CoG (being also the reference point) of CoG[m] = [5.67, 0.00, 1.34] yields a metacentric height GMxx of 3.73m, which clearly fits into the range specified in the literature.

With this information complete new calculations were done for the FPSO floater-mooring-system, with a correct hydrostatic stiffness and a more realistic vertical position of the CoG. The final results, obtained with these modifications are presented in the main part of this report.

⁴ Papanikolau, "Ship Design", p.262